



Efficient and selective approach to biomass-based amine by reductive amination of furfural using Ru catalyst

Hongtao Zou, Jinzhu Chen^{*}

College of Chemistry and Materials Science, Guangdong Provincial Key Laboratory of Functional Supramolecular Coordination Materials and Applications, Jinan University, Guangzhou 511443, China

ARTICLE INFO

Keywords:

Amine
Furfural
Hydrazine
Reductive amination
Ru catalyst

ABSTRACT

Reductive amination of furfural (**1a**) to furfurylamine (**2a**) was developed as a powerful and practical approach to biomass-based amine. Herein, Ru catalyst (Ru/BNC) supported on boron/nitrogen co-doped carbon (BNC) was reported for the reductive amination with hydrous hydrazine ($\text{N}_2\text{H}_4 \cdot \text{H}_2\text{O}$) as a nitrogen source and hydrazine as intermediate. Our mechanism investigation suggested rich Frustrated Lewis acid–base pairs (FLPs) on the BNC surface synergistically enhanced the activity of Ru catalyst. Moreover, quick formation rate of hydrazine intermediate and its moderate reactivity significantly improved **2a** selectivity. Under optimal conditions, Ru/BNC catalyst can highly efficiently and selectively promote **1a**/ N_2H_4 -to-**2a** transformation with **2a** yield exceeding 99%. Moreover, the role of nitrogen sources such as N_2H_4 , NH_3 and hydroxylamine on the **2a** selectivity was systematically investigated. Additionally, the developed Ru/BNC– N_2H_4 system was applicable to a wide range of aldehydes to give the desired primary amines in excellent to good yields (85–99%) in the reductive amination reaction.

1. Introduction

Primary amines are key building blocks for a variety of industrially-important productions such as pharmaceuticals, polymers, agricultural chemicals, dyes, and surfactants [1–5]. Among the developed synthetic strategies for primary amines, catalytic reductive amination of carbonyl compounds is the most powerful and practical approach by using hydrogen (H_2) as a reductant and ammonia (NH_3) as a nitrogen source [6–8]. However, these investigated carbonyl feedstocks are currently obtained from petrochemical processes by catalytic oxidation (for ketones) and catalytic hydroformylation (for aldehydes) [9–11]. In contrast to these fossil resource-derived carbonyl compounds, recently developed biorefinery process afforded renewable, readily available, and biomass-based carbonyl compounds such as furfural (**1a**), 5-hydroxymethylfurfural (**1b**), glycolaldehyde, 2,5-diformylfuran, vanillin and levulinic acid on a large scale [12–17]. Therefore, primary amines can be sustainably and extensively extended by the reductive amination reaction with biomass-based carbonyl compounds as the carbonyl feedstocks.

Very recently, reductive amination of **1a** with NH_3 to furfurylamine (**2a**) was investigated under H_2 atmosphere (Scheme 1a) [8]. The

obtained **2a** is a biomass-based primary amine with renewable nature, and is extensively used as an intermediate for the productions of drugs, pesticides and fibers [18]. Generally, the reported catalytic systems for **1a**-to-**2a** transformation were still very limited, which mainly includes Ru [8,9,19–25], Rh [26], Pd [27], Co [28,29], and Ni [30] with Ru as the most effective catalyst (Table S1, Supporting Information). NH_3 was extensively investigated as the most ideal nitrogen source for the **1a**-to-**2a** transformation due to its abundance and low cost. Nevertheless, the observed reaction network for **1a**/ NH_3 -to-**2a** transformation (Scheme 1a) is very complicated due to the occurrence and competition of various side-reactions, high reactivity of the *in-situ* formed furfurylimine (**5**) intermediate, and strong nucleophilicity of **2a** over NH_3 . Therefore, **2a** selectivity in the **1a**/ NH_3 -to-**2a** transformation is typically inhibited by: i) **1a** hydrogenation to furfuryl alcohol (**6**), ii) trimerization of **5** to furfurine (**14**), iii) **2a** hydrogenation to 2-tetrahydrofurfurylamine (**7**), and iv) secondary amine [*bis*(2-furanylmethyl)amine, **9**] formation [7,24]. Therefore, the development of highly selective and efficient catalytic system for **1a**-to-**2a** transformation remains a great challenging.

To address this issue, in this research, hydrous hydrazine ($\text{N}_2\text{H}_4 \cdot \text{H}_2\text{O}$) was developed as the nitrogen source for the reductive amination

^{*} Corresponding author.

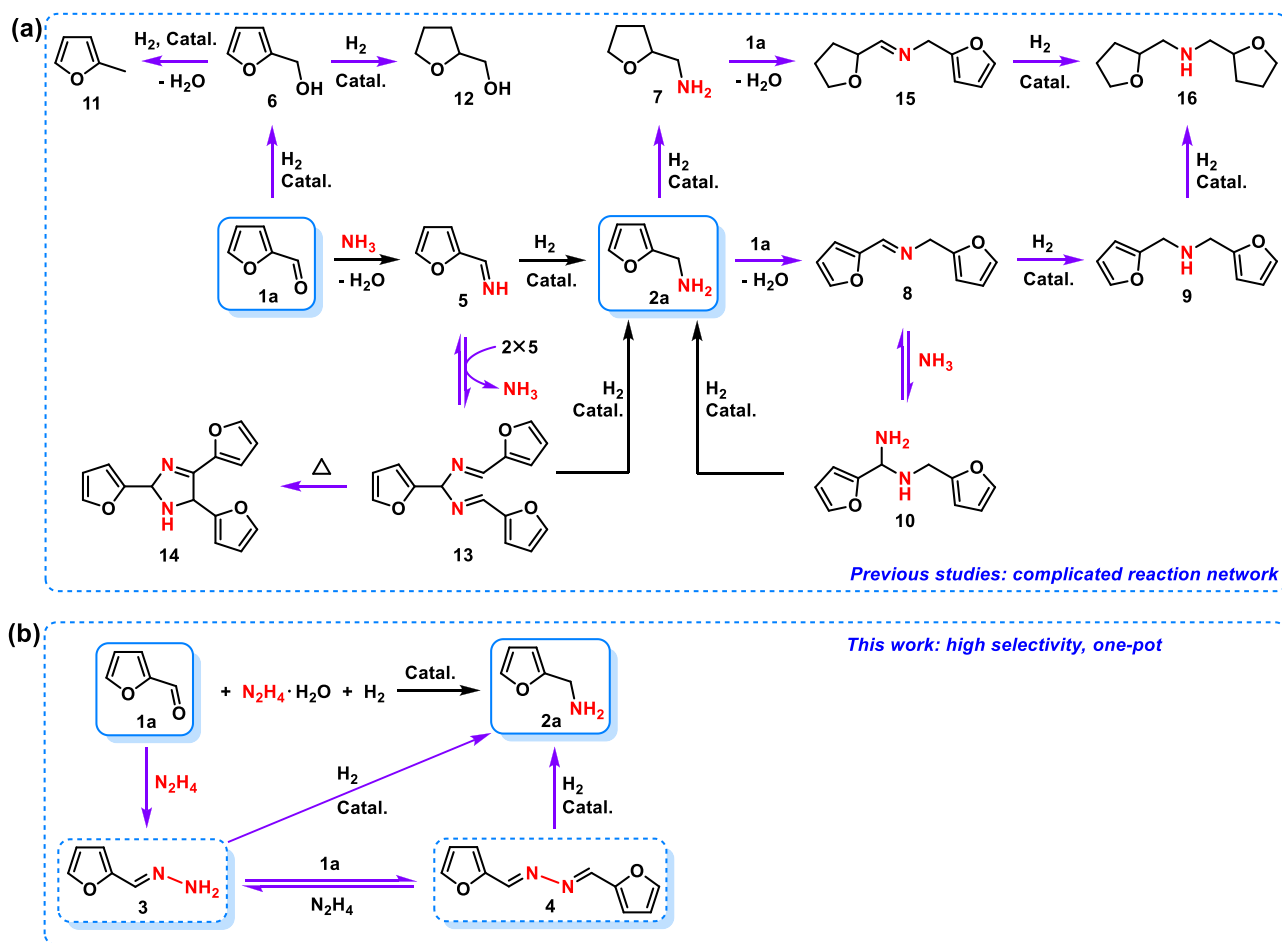
E-mail address: chenjz@jnu.edu.cn (J. Chen).

<https://doi.org/10.1016/j.apcatb.2022.121262>

Received 30 November 2021; Received in revised form 23 February 2022; Accepted 25 February 2022

Available online 2 March 2022

0926-3373/© 2022 Elsevier B.V. All rights reserved.



Scheme 1. Reaction networks for reductive amination of 1a to 2a with the nitrogen source of: (a) $\text{NH}_3 \cdot \text{H}_2\text{O}$ and (b) $\text{N}_2\text{H}_4 \cdot \text{H}_2\text{O}$

reaction of 1a to 2a with (2-furanylmethylene)hydrazine (3) and 1,2-bis(2-furanylmethylene)hydrazine (4) as the detected reaction intermediates (Scheme 1b). The use of $\text{N}_2\text{H}_4 \cdot \text{H}_2\text{O}$ as nitrogen source can completely eliminate 1a hydrogenation to 6 (Scheme 1a) owing to immediate and quantitative formation of 3/4 upon treatment 1a with $\text{N}_2\text{H}_4 \cdot \text{H}_2\text{O}$ even at ambient temperature [31,32]. Moreover, moderate reactivity of the intermediates 3/4 significantly enhanced 2a selectivity (Scheme 1b), thus effectively avoiding 5-induced side-reaction of trimerization (Scheme 1a). Finally, our mechanism investigation revealed that competitive adsorption of N_2H_4 and H_2 on the catalyst surface can appropriately reduce catalyst activity, which successively inhibits consecutive hydrogenation of 2a to 7 (Scheme 1a). Notably, side-product 9 (secondary amine) was undetected in the developed 1a/ N_2H_4 -to-2a system due to quick and full consumption of 1a at the initial reaction stage (Scheme 1b), although 9 was constantly observed in the 1a/ NH_3 -to-2a system (Scheme 1a).

In addition to the careful selection of nitrogen source, Ru catalyst was also rationally designed for the 1a/ N_2H_4 -to-2a transformation. Frustrated Lewis acid–base pairs (FLPs) was recently investigated as metal-free catalysts for H_2 activation [33]. For example, co-doping of electron-rich nitrogen (Lewis base) and electron-deficient boron (Lewis acid) on the surface of carbon promoted formation of surface FLPs, which can split H_2 to form H^+/H^- pairs [34]. In our case, we would like to endow the catalyst support such kind character in order to synergistically promote Ru site for H_2 activation. Therefore, lignin-derived boron/nitrogen co-doped carbon (BNC) with rich surface-immobilized FLPs was developed as the catalyst support in this research. As expected, the resulting Ru/BNC catalyst can highly efficiently and selectively promote 1a/ N_2H_4 -to-2a transformation with 2a yield exceeding

99%. Moreover, the developed Ru/BNC– N_2H_4 system was applicable to a wide range of aldehydes obtained from both biomass and fossil resource to give the corresponding primary amines in excellent to good yields (85–99%) via the reductive amination.

2. Experimental section

2.1. Preparation of catalyst

Synthesis of BNC. A mixture of lignin (1.0 g), boric acid (0.5 g), melamine (1.0 g) was ground in a mortar for 30 min. Carbonization was subsequently performed at 900 °C for 3 h with a temperature ramp rate of 3 °C min^{−1} under N_2 atmosphere. After cooling down to ambient temperature, the resulting black powder was thoroughly washed with distilled water and ethanol, and finally dried in an oven for 10 h at 80 °C under the vacuum to give BNC [35].

Synthesis of BC, NC and C. For comparison, the BC and NC were obtained in the same way of BNC without addition of melamine (for BC) and boric acid (for NC), respectively. Additionally, pristine carbon (C) was obtained by directly pyrolyzing lignin under the same synthetic conditions of BNC.

Synthesis of Ru nanocatalyst. Ru catalyst was prepared by traditional wet chemical impregnation and reduction method [36]. In a typical procedure to Ru/BNC, BNC (100 mg) was initially dispersed in methanol (MeOH, 50 mL) and followed by addition of RuCl_3 solution (0.01 M in MeOH, 2.0 mL) with vigorous stirring. After stirring for 6 h, fresh prepared NaBH_4 solution (50 mg NaBH_4 in 1.0 mL MeOH) was rapidly injected into the above mixture, the obtained mixture was then continuous stirring for another 10 min. Finally, the black sample was

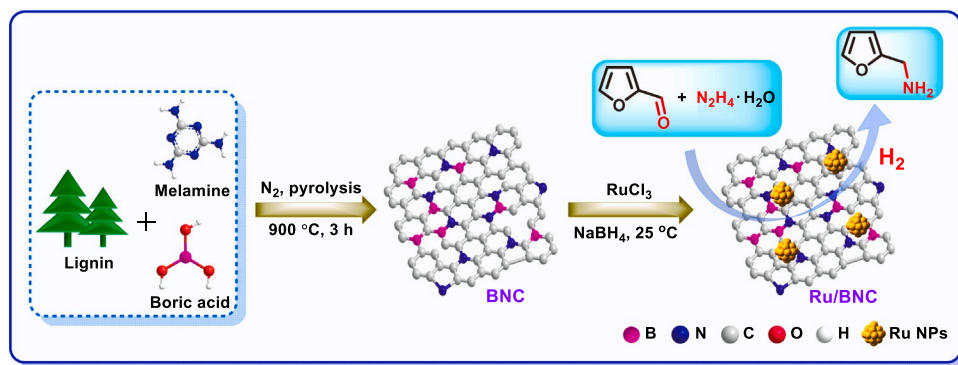


Fig. 1. Scheme of the Ru/BNC preparation and its promoted reductive amination of 1a with $N_2H_4 \cdot H_2O$ to 2a.

centrifuged, washed with MeOH for three times, and dried under vacuum at $40\text{ }^\circ\text{C}$ overnight to give Ru/BNC (Ru, 1.8 wt%).

For comparison purpose, Ru NPs, Ru/C, Ru/NC, and Ru/BC catalysts

were synthesized by the same synthetic procedure of Ru/BNC. In addition, M/BNC (M = Fe, Co, Ni, Cu, Rh and Pd) catalysts were also prepared by the same method.

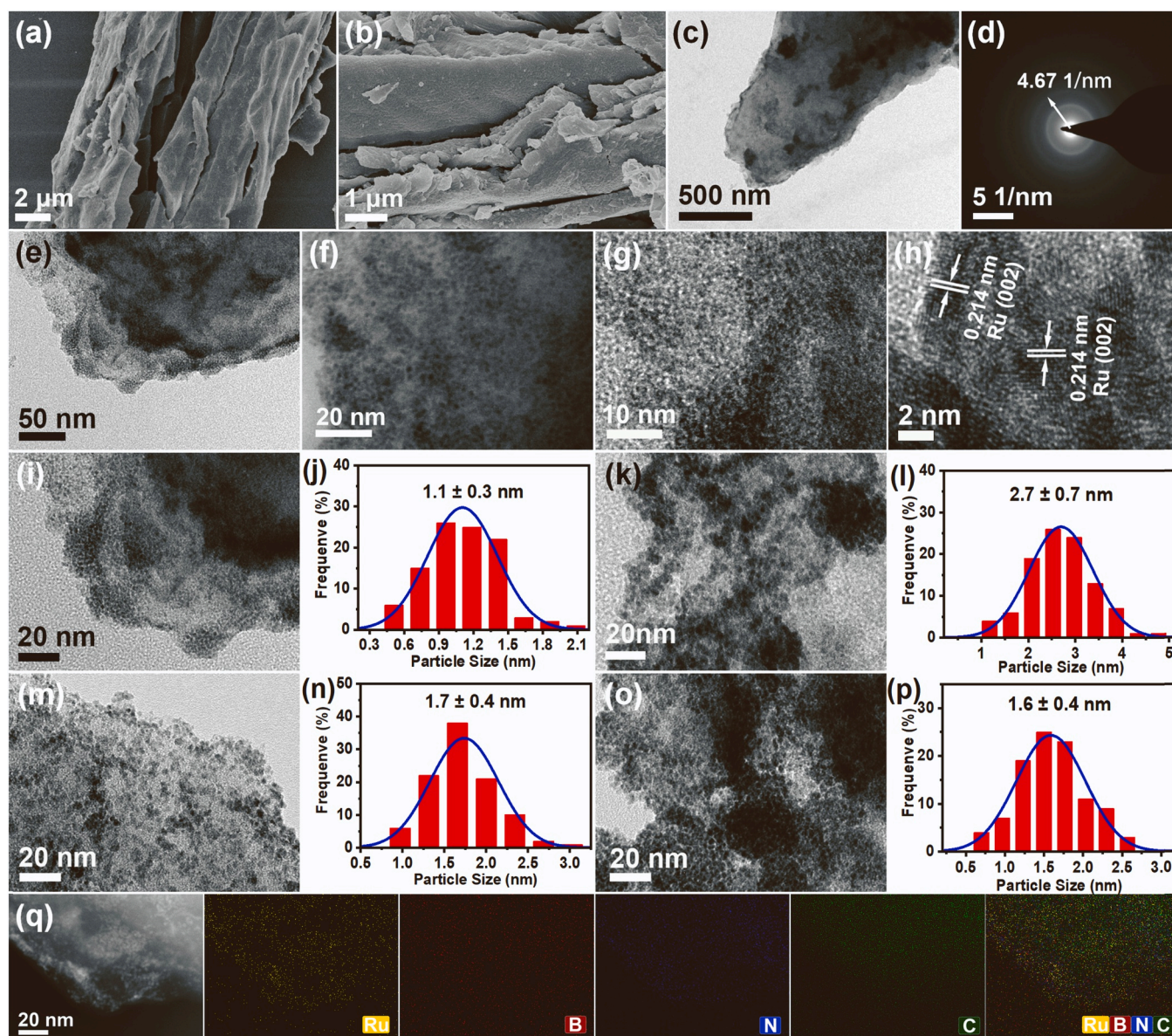


Fig. 2. Ru/BNC: (a,b) SEM images, (c,e,f) TEM images, (d) SAED pattern, and (g,h) HRTEM images. TEM images and the corresponding histograms of (i,j) Ru/BNC, (k,l) Ru/C, (m,n) Ru/NC, and (o,p) Ru/BC. (q) HAADF-STEM image of Ru/BNC and the corresponding elemental mappings.

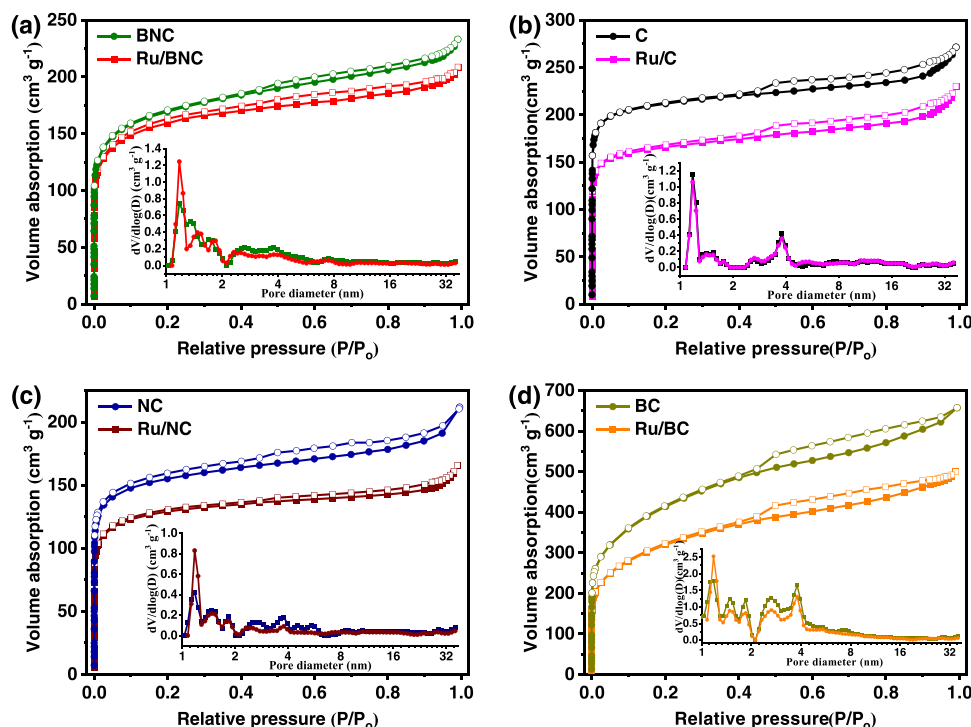


Fig. 3. N_2 adsorption-desorption isotherms of (a) BNC and Ru/BNC, (b) C and Ru/C, (c) NC and Ru/NC, (d) BC and Ru/BC. Insets at the bottom show the corresponding pore size distributions.

2.2. Reductive amination of furfural

Reaction apparatus for testing the reductive amination of furfural is the same as the previously reported [37,38]. Typically, Ru/BNC (10 mg), **1a** (0.12 mmol), MeOH (2.0 mL) and $N_2H_4 \cdot H_2O$ (0.48 mmol, 4 equivalents to **1a**) were added into a 25 mL stainless autoclave reactor. Then H_2 was slowly purged into the autoclave for three times to replace the air inside the autoclave reactor. H_2 (2.0 MPa) was finally charged into the reactor. The reaction was performed for 16 h at 80 °C with vigorous stirring. After cooling down to ambient temperature, the resulting reaction mixture was diluted with MeOH (10 mL), filtered and analyzed by GC and GC-MS to determine substrate conversion and product yield. The isolated product was further characterized by NMR. The substrate conversion and product yield were calculated using the following equations:

$$\text{Conversion (\%)} = \frac{\text{mole of substrate consumed}}{\text{mole of initial substrate}} \times 100\%$$

$$\text{Yield (\%)} = \frac{\text{mole of product formed}}{\text{mole of initial substrate}} \times 100\%$$

2.3. Characterization methods

The morphology, nanoparticle size, and elemental distribution of Ru samples were observed by scanning electron microscopy (SEM, Ultra-55), transmission electron microscope (TEM, JEOL, JEM-2100 F), and high-angle annular dark-field scanning transmission electron microscopy (HAADF-STEM, Talos F200X, FEI, USA) with an energy dispersive X-ray (EDX) analysis system operated at 200 kV. The BET specific surface area measurements were performed with N_2 adsorption-desorption isotherms at liquid-nitrogen temperature (77 K) using automatic volumetric adsorption equipment (Autosorb-iQ, Quantachrome). Before the analysis, the samples were evacuated at 250 °C for 6 h. Powder X-ray diffraction (XRD) patterns were measured by a Rigaku MiniFlex-600 X-ray diffractometer using Cu K α radiation (40 kV, 40 mA). Raman spectra

were obtained from a Raman spectrometer (LabRAM HR Evolution) using a 532 nm laser. X-ray photoelectron spectroscopy (XPS) measurements were collected on a Thermo Scientific K-Alpha⁺ system with an Al K α source. Inductively coupled plasma-atomic emission spectroscopy (ICP-AES) measurements were performed on a Thermo iCAP 7000 SERIES instrument to measure the content of Ru. The product was quantified by a FuLi GC-9790 (II) equipped with a KB-5 column (30 m \times 0.32 mm \times 0.25 μ m) connected to flame ionization detector (FID). The structural characterizations of the reductive amination products were studied using gas chromatography-mass spectrometer analysis (GCMS-QP2020) and nuclear magnetic resonance spectrometers (NMR, Bruker AV III 300).

3. Results and discussion

3.1. Catalyst preparation

In this research, lignin-derived boron/nitrogen co-doped carbon (BNC) was prepared by calcination a mixture of lignin, boric acid and melamine at 900 °C under N_2 atmosphere (Fig. 1). The BNC-supported Ru catalyst (Ru/BNC) was then prepared by a wet chemical impregnation of BNC with $RuCl_3$ followed by $NaBH_4$ reduction. For comparison purpose, various supports such as lignin-derived carbon (C), lignin-derived N doped carbon (NC), and lignin-derived B doped carbon (BC) were respectively prepared with the similar synthetic procedure of BNC. The resulting Ru catalysts involving Ru/C, Ru/NC and Ru/BC were subsequently obtained with the same preparation method of Ru/BNC.

3.2. Catalyst characterization

The morphology of various Ru samples was initially investigated and compared using scanning electron microscopy (SEM) and transmission electron microscopy (TEM). SEM images of Ru/BNC sample showed a layered platelet-like architecture (Fig. 2a,b). TEM images of the Ru/BNC exhibited homogeneously dispersed ultrafine Ru nanoparticles (NPs) with a mean NPs size of 1.1 nm on the BNC support (Fig. 2c-j). The

Table 1
Porosity properties of investigated samples.

Samples	S_{BET}^a [m ² g ⁻¹]	S_{micro}^b [m ² g ⁻¹]	S_{meso}^c [m ² g ⁻¹]	$D_{\text{micro}}/D_{\text{meso}}^d$ [nm]	V_{total}^e [cm ³ g ⁻¹]	$V_{\text{micro}}/V_{\text{meso}}^f$ [cm ³ g ⁻¹]
BNC	629.1	479.0	150.1	1.2/3.8	0.36	0.20/ 0.16
Ru/BNC	591.9	487.2	104.7	1.2/3.8	0.32	0.20/ 0.12
C	828.3	742.4	85.9	1.2/3.8	0.42	0.29/ 0.13
Ru/C	643.3	550.2	93.1	1.2/3.8	0.36	0.24/ 0.12
NC	587.2	501.4	85.8	1.2/3.8	0.33	0.20/ 0.13
Ru/NC	490.2	430.9	59.3	1.2/3.8	0.26	0.18/ 0.08
BC	1456.5	748.4	708.1	1.2/3.8	1.02	0.34/ 0.68
Ru/BC	1133.7	624.4	509.3	1.2/3.8	0.76	0.28/ 0.48
Recovered Ru/BNC	510.0	308.3	201.7	1.2/2.8	0.41	0.13/ 0.27

^a Specific BET surface area

^b micropore area

^c mesopore area

^d diameters of micropore and mesopore

^e total pore volume

^f pore volumes of micropore and mesopore

selected-area electron diffraction (SAED) pattern of the Ru/BNC (Fig. 2d) shows weak diffraction rings, clarifying the ultrasmall size with low crystallinity of Ru NPs [39]. The diffraction ring radius was determined to be 4.67 1/nm, corresponding to the (002) lattice plane of Ru, which thus confirms the successful formation of low crystalline Ru NPs on the BNC support. Furthermore, the high-resolution TEM (HRTEM) images of Ru/BNC (Fig. 2g,h) further confirmed the crystal plane of Ru (002) [39], which is consistent with the results from its SAED analysis. Finally, the High-Angle Annular Dark-Field Scanning Transmission Electron Microscopy (HAADF-STEM) and Energy Dispersive X-ray Spectroscopy (EDX) elemental mapping of Ru/BNC (Fig. 2q) demonstrated uniform dispersion of Ru, B, N, and C on the Ru/BNC surface.

In contrast to Ru/BNC, Ru NPs are roughly dispersed on pure C support for Ru/C sample with an observed aggregation in large particle size of 2.7 nm (Fig. 2k,l). For Ru/NC and Ru/BC samples, Ru NPs well distributed on NC and BN with a much smaller Ru particle size of 1.7 (Fig. 2m,n) and 1.6 nm (Fig. 2o,p), respectively, suggesting an excellent immobilization effect of the doped heteroatom in the supports (NC and BC) on the Ru NPs.

Fig. 3 shows the N₂ sorption isotherms and the resulting pore size distributions of the investigated samples, their porosity properties are listed in Table 1. For BNC support, a steep uptake of N₂ adsorption at a

relative pressure (P/P_0) of 0–0.08 indicates typical I isotherm feature [40]. Moreover, an observed hysteresis loop at $P/P_0 > 0.4$ demonstrates a combined character of type I and IV isotherms, suggesting the existence of both micropores and mesopores for BNC. The specific BET surface area is 629.1 m² g⁻¹ for BNC and reduces to 591.9 m² g⁻¹ for the resulting Ru/BNC upon the loading of Ru NPs (Table 1), suggesting partial block of the BNC pores by Ru NPs in the Ru/BNC. Generally, both BNC and Ru/BNC exhibit micropore-dominated hierarchically micro–mesoporous architecture. Notably, heteroatom doping affects surface area of the resulting support [41]. For example, N-doping leads to a significantly reduced surface area to 587.2 m² g⁻¹ for NC if compared with 828.3 m² g⁻¹ for the pristine C support. While, B-doping results in remarkably increased surface area to 1456.5 m² g⁻¹ for BC. Therefore, Ru/BC shows the highest specific surface area (1133.7 m² g⁻¹) among the developed Ru samples. Generally, all of the Ru samples are rich in micropore with limited mesopore.

Crystal structures of various samples were characterized by X-ray diffraction (XRD) (Fig. 4a). The XRD patterns of all the as-prepared samples exhibit similar diffraction patterns with a broad peak at 23° and a weak peak at 44°, which are respectively assigned to the (002) and (100) planes of *sp*²-hybridized graphite carbon [42]. However, the graphitic carbon (002) diffraction peaks from NC, BC, and BNC slightly shifted to the higher angles when compared with pristine C, which might result from the disordered graphitic structure by heteroatom-doping [43,44]. Notably, no characteristic peaks of metallic Ru species were detected from Ru/BNC, suggesting highly dispersed Ru NPs with ultrasmall size and low crystallinity on the BNC support. Moreover, Ru/BNC exhibits relatively weaker and broader peaks at 23° and 44° when compared with its BNC support, indicating a lower crystallization degree of the highly dispersed Ru on the BNC surface. Generally, our XRD results are consistent with the above TEM analyses, confirming the formation of Ru NPs with an ultrasmall size and low crystallinity over Ru/BNC. Similar results were also observed with other Ru samples including Ru/C, Ru/NC, and Ru/BC.

The Raman spectroscopy was used to probe the effect of doped B and N on the graphitization degree of the supports (Fig. 4b). All of the as-synthesized supports exhibit two typical bands at around 1330 cm⁻¹ and 1580 cm⁻¹, which are respectively indexed to the D peak from disordered carbon (*sp*³) and the G peak from graphite carbon (*sp*²) [35]. The graphitization degree of these carbon supports was evaluated by the intensity ratio of the D band to G band (I_D/I_G). The I_D/I_G ratios are 1.07 for C, 1.08 for NC, 1.13 for BC, and 1.19 for BNC, respectively, demonstrating increased defects in the graphite-like layer upon heteroatom-doping. Therefore, incorporation of heteroatoms such as N and B into the carbon skeleton reduced the graphitic structure units, increased disorder in the matrix of graphitic carbon [42]. Generally, our Raman analysis is in line with the XRD results.

X-ray photoelectron spectroscopy (XPS) characterizations were performed to determine the surface states and chemical environment of the as-synthesized Ru catalysts (Fig. 5, Table S2 and S3, Supporting

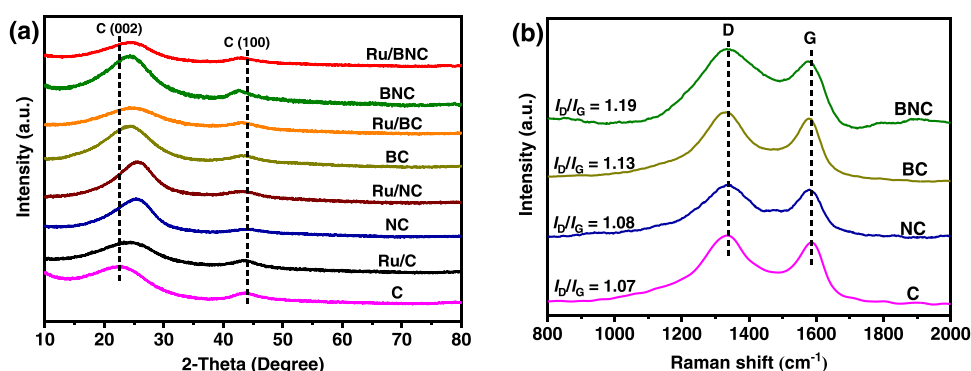


Fig. 4. (a) XRD patterns of C, Ru/C, NC, Ru/NC, BC, Ru/BC, BNC and Ru/BNC. (b) Raman spectra of C, NC, BC and BNC.

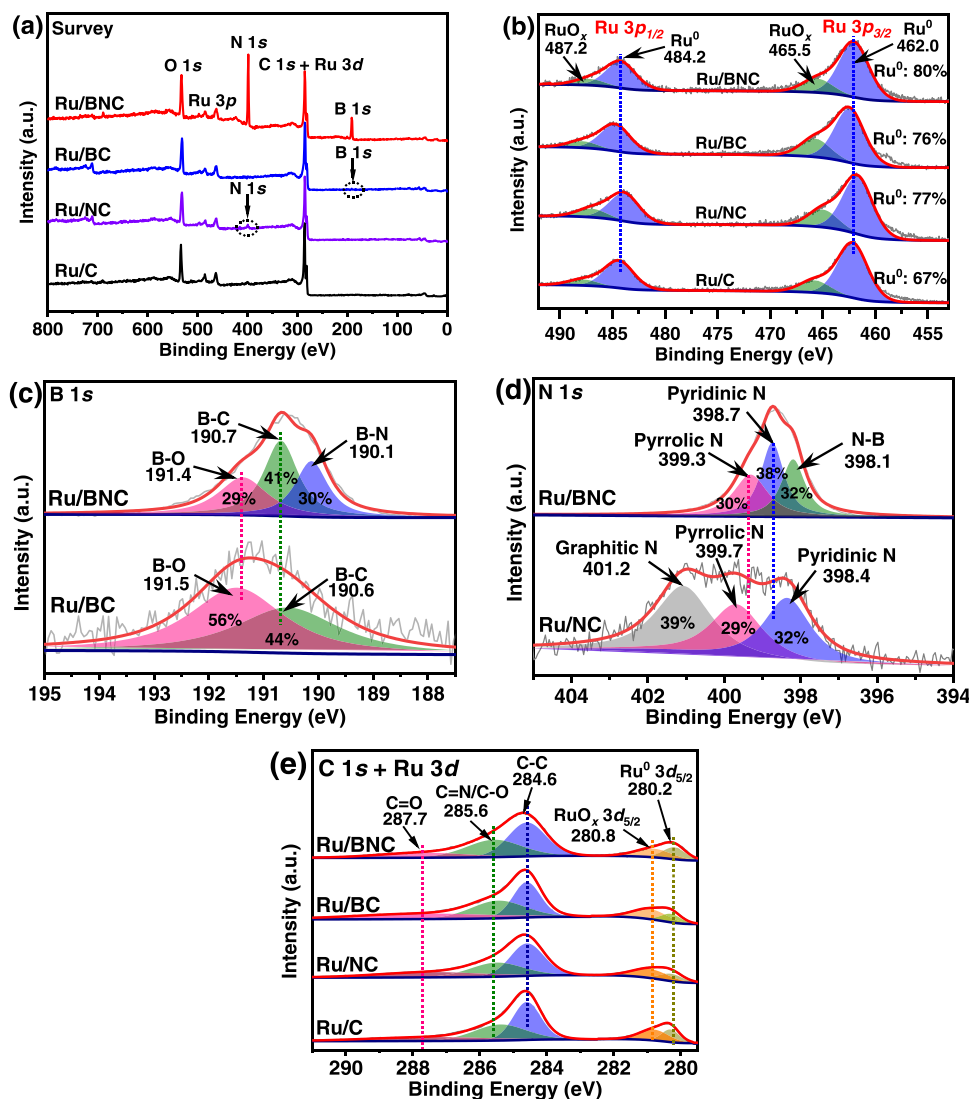


Fig. 5. (a) The XPS survey, (b) Ru 3p XPS, (c) B 1s XPS, (d) N 1s XPS, and (e) C 1s XPS of the investigated samples.

Information). The XPS survey of Ru/BNC shows the presence of main elements including Ru (2 atom%), C (49 atom%), O (11 atom%), B (19 atom%), and N (19 atom%) (Fig. 5a). In sharp contrast, a significantly reduced N content (3 atom%) in Ru/NC and B content (3 atom%) in Ru/BC were observed. The above result thus suggested that co-doping B and N can efficiently enhance their contents in the BNC sample.

Because of the overlap of the binding energies between Ru 3d XPS and C 1s XPS (284.6 eV), Ru 3p XPS of various Ru samples were detected and analyzed despite of their reduced signal/noise ratio [45]. As shown in Fig. 5b, two doublets for Ru 3p_{3/2} and Ru 3p_{1/2} in Ru/BNC were clearly observed, which can be deconvoluted into four peaks, corresponding to metallic Ru⁰ (462.0 eV in Ru 3p_{3/2} and 484.2 eV in Ru 3p_{1/2}) and RuO_x (465.5 eV in Ru 3p_{3/2} and 487.2 eV in Ru 3p_{1/2}) species with Ru⁰ as the major species (80%) [45,46]. The observed RuO_x species on the Ru/BNC surface is presumably caused by surface oxidation of Ru⁰ species upon its exposure to air. Generally, Ru 3p XPS of Ru/C, Ru/NC and Ru/BC are similar to Ru/BNC (Fig. 5b). However, the co-presence of B and N in Ru/BNC increases the relative percentage of Ru⁰ species. Among the investigated Ru samples, Ru/BNC shows the highest relative content of Ru⁰ (80%) species; while Ru/C exhibits the lowest relative percentage of Ru⁰ (67%) species. Therefore, the co-doping of heteroatoms B and N in the BNC is presumably beneficial for immobilization of active Ru⁰ species by inhibiting its further oxidation.

The B 1s XPS of Ru/BNC can be divided into three peaks at 190.1 eV

(assigned to B–N, 30%), 190.7 eV (assigned to B–C, 41%) and 191.4 eV (assigned to B–O, 29%), with B–C species as prevailing species (Fig. 5c) [47,48]. The presence of B–N species suggests the strong bonding between N and B atoms and the formation of FLPs on the Ru/BNC surface. In the case of Ru/BC, only two peaks were observed at 190.6 and 191.5 eV, respectively corresponding to B–C and B–O species.

The N 1s XPS of Ru/BNC exhibits three peaks at 398.1 eV (indexed to N–B, 32%), 398.7 eV (indexed to pyridinic N, 38%), and 399.2 eV (indexed to pyrrolic N, 30%) (Fig. 5d). For Ru/NC, the peak related to B–N species was unobserved; while, Ru/NC shows a new peak located at 401.2 eV, corresponding to graphite N species [49]. The above results thus indicate that the introduced B atom can change the type of the doped N species, by yielding new N–B species instead of graphite N [50–52].

The C 1s XPS of Ru/BNC can be well deconvoluted into three signals, respectively corresponding to C–C (284.4 eV), C=N/C–O (285.6 eV), and C=O (287.6 eV) (Fig. 5e) [53]. The C 1s XPS of Ru/C, Ru/NC, and Ru/BC are almost the same as Ru/BNC. The above results demonstrate that heteroatom doping shows a limited effect on the carbon structure for the supports.

Therefore, our B 1s and N 1s XPS analyses of Ru/BNC reveal that co-doping B and N leads to formation of B–N species, which may promote the generation of B–N FLPs on the Ru/BNC surface. The Ru 3p XPS characterization of Ru/BNC confirms surface metallic Ru⁰ species as

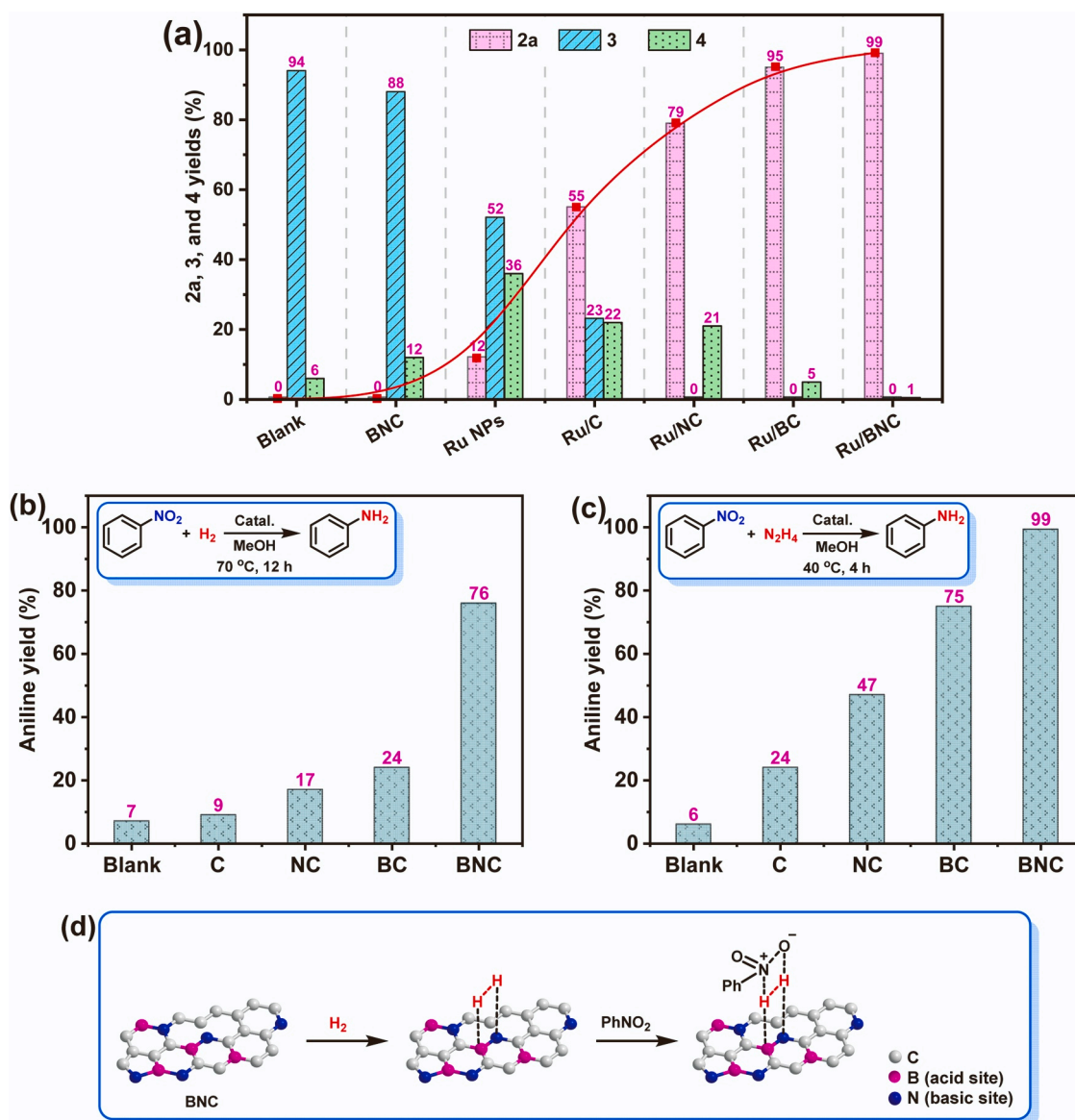


Fig. 6. (a) Reductive amination of **1a** to **2a** over various catalysts; (b) hydrogenation and (c) transfer hydrogenation of nitrobenzene to aniline with various supports; (d) proposed mechanism for FLPs-promoted H₂ activation on the BNC surface. Reaction conditions: (a) catalysts (10 mg, 1.1 mol% Ru relative to **1a**), **1a** (0.12 mmol), N₂H₄·H₂O (0.24 M in 2.0 mL MeOH, 4 equivalents to **1a**), H₂ (2.0 MPa), 80 °C, 16 h; (b) nitrobenzene (0.12 mmol), supports (10 mg), H₂ (2.0 MPa), 70 °C, 12 h; (c) nitrobenzene (0.12 mmol), supports (10 mg), N₂H₄·H₂O (0.24 M in 2.0 mL MeOH, 4 equivalents to nitrobenzene), N₂ (2.0 MPa), 40 °C, 4 h.

major species (80%) for hydrogenation step. While, surface RuO_x species may presumably function as Lewis acid site for amination (condensation) step.

3.3. Reductive amination of furfural to furfurylamine

Various Ru catalysts were previously investigated for the reductive amination of **1a** with NH₃ for **2a** formation under pressurized H₂ (Table S1), and a complicated reaction networks were observed for the reaction (Scheme 1a). In this research, the above developed Ru-based nanocatalysts were initially screened for the reductive amination of **1a** to **2a** with N₂H₄·H₂O as nitrogen source under H₂ atmosphere at 80 °C in methanol (Scheme 1b and Fig. 6a). Blank experiment demonstrated that only intermediates **3** and **4** were produced in the absence of any catalysts. Moreover, catalyst support BNC by itself cannot promote the transformations of **3** and **4** to the desired **2a** under the investigated conditions. In contrast, 12% yield of **2a** was obtained from pure Ru NPs, indicating the key role of metallic Ru on the hydrogenation.

Immobilization of Ru NPs on various catalyst supports significantly enhanced their catalytic activity by producing **2a** in 55–99% yields. Among various developed Ru catalysts, Ru/BNC demonstrated an excellent activity and selectivity by affording > 99% yield of **2a**, suggesting outstanding hydrogenative activity of Ru/BNC towards both **3** and **4**. In contrast, a physical mixture of Ru NPs and BNC produced 25% yield of **2a** (Fig. S1, Supporting Information). Therefore, the excellent catalytic performance of Ru/BNC is presumably attributed to the synergistic effect between the supported ultrafine Ru NPs (1.1 nm) and BNC support with FLPs feature.

Our controlled experiments confirmed inactive of BNC support towards hydrogenation of **3** and **4** to **2a**. To understand the influence of FLPs from BNC support on the hydrogenation, hydrogenation and transfer hydrogenation of nitrobenzene to aniline were then respectively investigated as model reactions over various supports. Fig. 6b shows nitrobenzene hydrogenation to aniline with H₂ as hydrogen source at 70 °C in methanol with various obtained supports as catalysts. Negligible aniline yield (7%) was obtained under catalyst free conditions, and

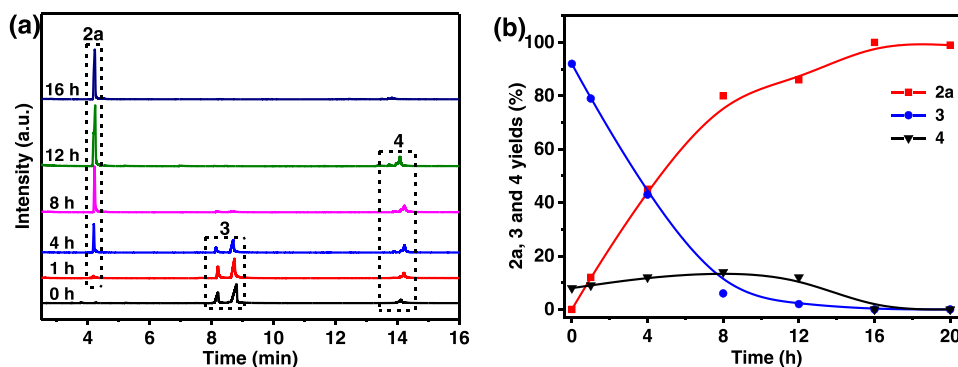


Fig. 7. Ru/BNC-promoted reductive amination of **1a** with $\text{N}_2\text{H}_4\cdot\text{H}_2\text{O}$ for **2a** synthesis: (a) time-dependent GC-MS analysis and (b) the corresponding reaction time profile vs. product distribution. Reaction conditions: **1a** (0.12 mmol), Ru/BNC (10 mg, 1.8 wt% Ru, 1.1 mol% Ru relative to **1a**), $\text{N}_2\text{H}_4\cdot\text{H}_2\text{O}$ (0.24 M in 2.0 mL MeOH, 4 equivalents to **1a**), H_2 (2.0 MPa), 80°C .

C support cannot promote nitrobenzene hydrogenation. NC and BC slightly increased aniline yield to 17% and 24%, respectively. In sharp contrast, a significantly enhanced aniline yield to 76% was obtained with BNC. In addition to hydrogenation, transfer hydrogenation of nitrobenzene with $\text{N}_2\text{H}_4\cdot\text{H}_2\text{O}$ to aniline was investigated by using various supports at 40°C . Again, BNC exhibited superior activity over other supports by giving quantitative aniline yield under the investigated conditions (Fig. 6c).

Our B 1s and N 1s XPS analyses from Ru/BNC demonstrate the formation of B–N species on the catalyst surface (Fig. 5c,d), which may lead to the generation of B–N-based FLPs on the Ru/BNC surface (Fig. 6d). Previously, molecular FLPs was investigated as metal-free catalyst for H_2 splitting [54,55]. In our case, these B–N-based Lewis acid–base pairs are presumably separated by an appropriate distance but in a close and suitable distance to each other, which thus avoids their collapse by mutual neutralization [56,57]. We believe that these immobilized

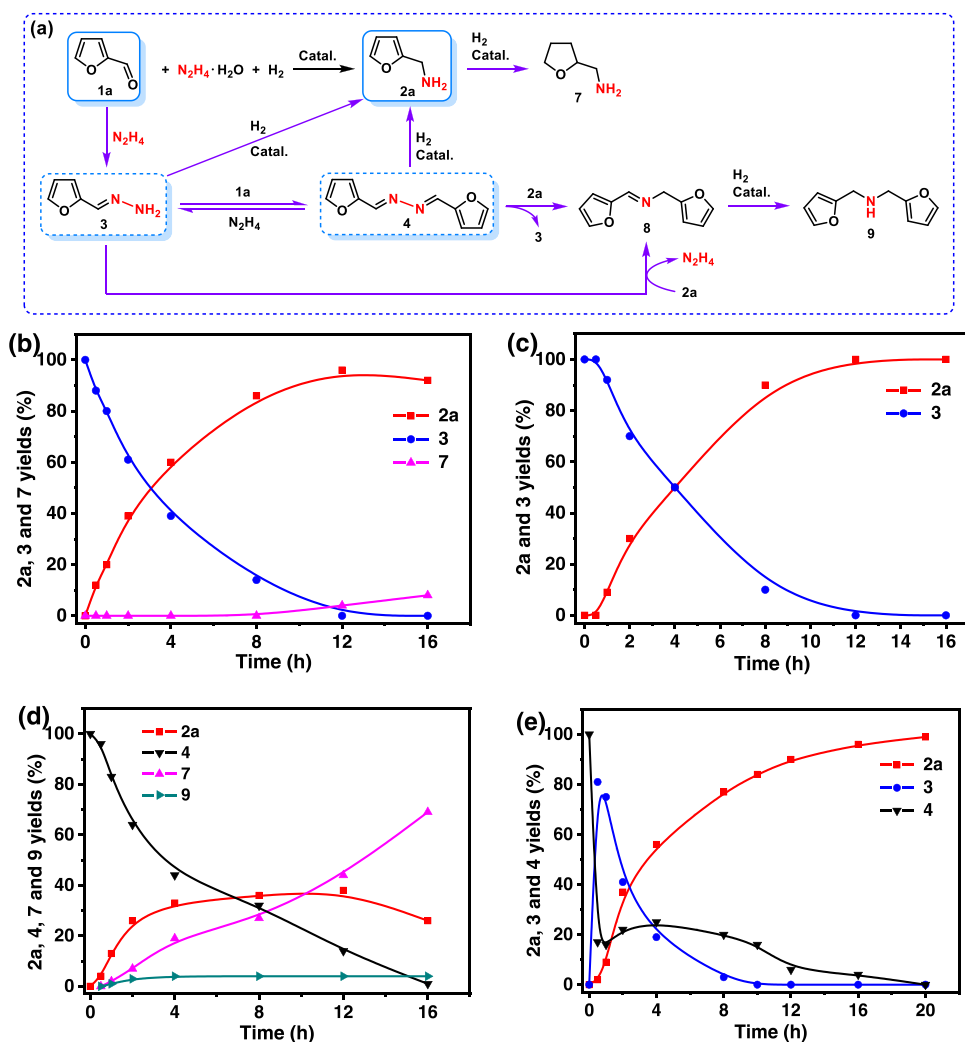


Fig. 8. (a) Reaction network for Ru/BNC-promoted reductive amination. Ru/BNC-promoted reaction time profile vs. product distribution: (b) direct hydrogenation of **3** to **2a**, (c) **3** hydrogenation to **2a** in the presence of $\text{N}_2\text{H}_4\cdot\text{H}_2\text{O}$, (d) direct hydrogenation of **4** to **2a**, and (e) **4** hydrogenation to **2a** in the presence of $\text{N}_2\text{H}_4\cdot\text{H}_2\text{O}$. Reaction conditions: (b and d) **3** or **4** (0.12 mmol), Ru/BNC (10 mg, 1.8 wt% Ru, 1.1 mol% Ru relative to **3** or **4**), H_2 (2.0 MPa), 80°C ; (c and e) $\text{N}_2\text{H}_4\cdot\text{H}_2\text{O}$ (0.24 M in 2.0 mL MeOH, 4 equivalents to substrate) was respectively added into (b) and (d).

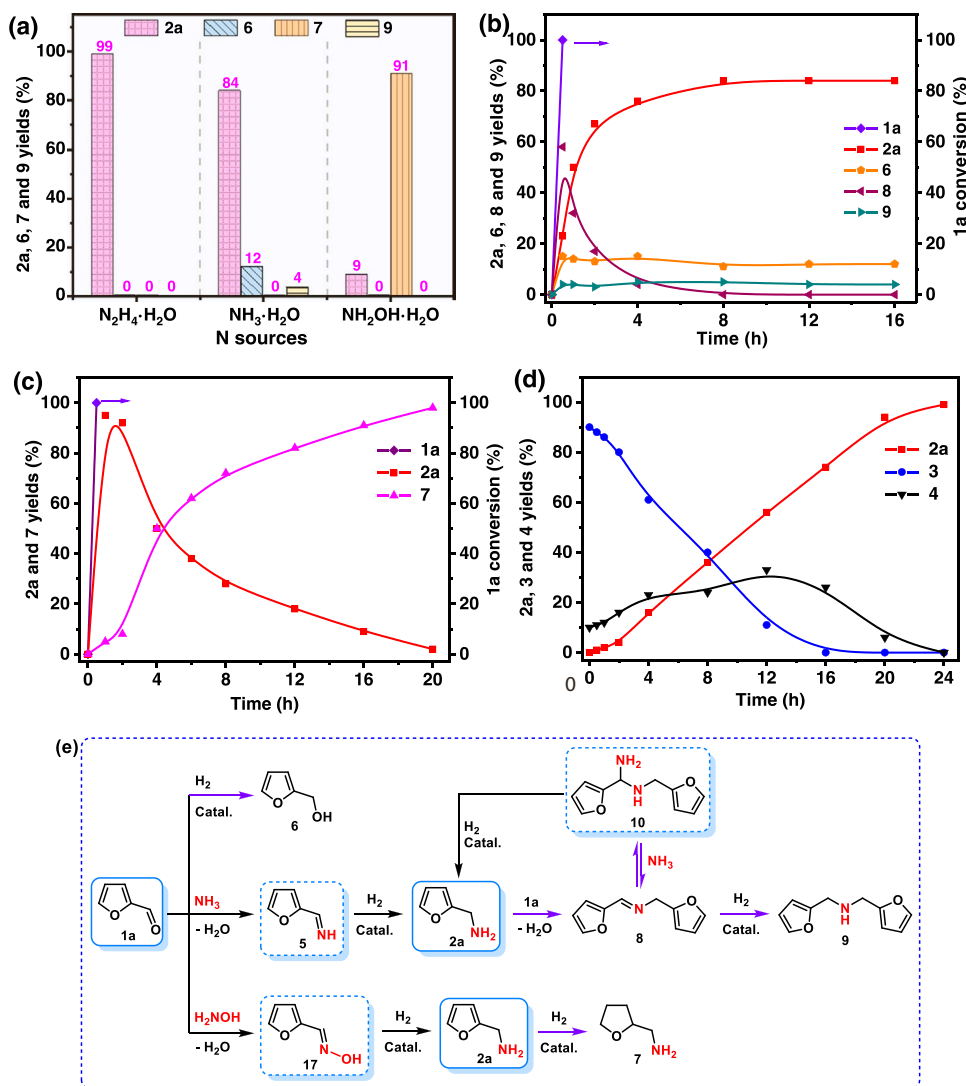


Fig. 9. (a) Effect of nitrogen source on the reductive amination of **1a** over Ru/BNC catalyst. Ru/BNC-promoted reaction time profile vs. product distribution: (b) reductive amination of **1a** with $\text{NH}_3\cdot\text{H}_2\text{O}$, (c) reductive amination of **1a** with $\text{H}_2\text{NOH}\cdot\text{H}_2\text{O}$, (d) reductive amination of **1a** with a mixture of $\text{NH}_3\cdot\text{H}_2\text{O}$ and $\text{N}_2\text{H}_4\cdot\text{H}_2\text{O}$ (1:1 molar ratio). (e) Reaction network for Ru/BNC-promoted reductive amination of **1a** with $\text{NH}_3\cdot\text{H}_2\text{O}$ and $\text{H}_2\text{NOH}\cdot\text{H}_2\text{O}$. Reaction conditions: **1a** (0.12 mmol), Ru/BNC (10 mg, 1.8 wt % Ru, 1.1 mol% Ru relative to **1a**), H_2 (2.0 MPa), 80°C , nitrogen source (0.24 M in 2.0 mL MeOH, 4 equivalents to **1a**).

B-N-based FLPs may function as molecular FLPs for catalytic H_2 activation/splitting and then promote nitrobenzene hydrogenation (Fig. 6d). In the case of Ru/BNC-catalyzed reductive amination of **1a**, we think these FLPs on the catalyst surface may play a positive role in the hydrogenation step, thus leading to an enhanced catalytic performance over other investigated Ru catalysts.

The effect of metallic site on the reductive amination was investigated by BNC-supported various transition metal catalysts M/BNC ($\text{M} = \text{Fe}, \text{Co}, \text{Ni}, \text{Cu}, \text{Rh}$ and Pd ; Fig. S2, Supporting Information). Generally, M/BNC catalysts, composed of earth abundant transition metals ($\text{M} = \text{Fe}, \text{Co}, \text{Ni}$ and Cu), cannot promote the transformations of the intermediates **3** and **4** to the desired **2a** under the investigated conditions. In the cases of Pd/BNC and Rh/BNC catalysts, low **2a** yields of 18% and 53% were respectively obtained due to low activity/selectivity of the catalysts to the desired **2a**.

3.4. Reaction pathway of the reductive amination

Scheme 1b shows the proposed reaction pathway of the Ru/BNC-promoted hydrogenative amination under the optimized conditions by using time-dependent gas chromatography-mass spectrometry (GC-MS) (Fig. 7a). Both **3** (m/z 110, Fig. S3, Supporting Information) and **4** (m/z 188, Fig. S4, Supporting Information) were observed to be formed initially and consumed later in the interval of reaction time, thus

suggesting a detectable intermediate feature of **3** and **4**. However, **2a** (m/z 97, Fig. S5, Supporting Information) was detected to smoothly increase with the reaction time, corresponding to the final product character. Notably, *cis-trans* isomerism of both **3** and **4** were clearly observed by the GC-MS analysis (Fig. 7a). Fig. 7b plots the resulting profiles of reaction time vs. product distribution according to Fig. 7a. Both **3** and **4** quantitatively and immediately formed upon treatment **1a** with $\text{N}_2\text{H}_4\cdot\text{H}_2\text{O}$ (Fig. 7b). **3** yields steeply decreased from 92% to 2% at the initial reaction time of 12 h; while, **2a** yield accordingly and proportionally increased to 86% at this stage. In contrast, **4** yields slightly fluctuated between 8% and 14% at the initial 12 h. The above observations thus demonstrated an increased **2a** yield at the expense of the **3** conversion, suggesting a direct hydrogenation of **3** to **2a** at the initial stage. Finally, a **4**-to-**2a** transformation initiated beyond this time, leading to > 99% yield of **2a** at 16 h. The above reaction pathway thus suggested an *in-situ* formed intermediate behaviors of monohydrazone **3** and dihydrazone **4** (Scheme 1b).

3.5. Effect of hydrazine on furfurylamine selectivity

To understand the effect of $\text{N}_2\text{H}_4\cdot\text{H}_2\text{O}$ on **2a** formation, both **3** and **4** were prepared and respectively introduced into the reductive amination reaction as starting reagents (Fig. 8a). Fig. 8b shows the resulting profiles of reaction time vs. product distribution for direct hydrogenation of

3 with Ru/BNC catalyst under pressurized H_2 . As expected, **2a** yield smoothly increased with a steady decline of **3** concentration, **2a** yield finally increased to a maximum of 96% at 12 h with a full conversion of **3**. However, 4% yield of **7** (Fig. 8b and S6, Supporting Information) was also observed at this stage. Prolonged reaction time to 16 h further decreased **2a** yield to 92% with an enhanced **7** yield to 8%. The observed product **7** is attributed to further hydrogenation of furan ring in **2a** (Fig. 8a), thus leading to a reduced **2a** selectivity. Evidently, direct hydrogenation of **3** resulted in a decreased **2a** selectivity if compared with reductive amination of **1a** with excess amount of $N_2H_4 \cdot H_2O$ (Fig. 7).

To probe the presence of $N_2H_4 \cdot H_2O$ on the **2a** selectivity, direct hydrogenation of **3** was performed in the existence of 4 equivalents of $N_2H_4 \cdot H_2O$ for comparison purpose. Interestingly, **3** was highly selectively and quantitatively converted into **2a** in > 99% yield at 16 h; moreover, product **7** was unobserved to any detectable extents (Fig. 8c). This result suggested the contribution of additionally introduced $N_2H_4 \cdot H_2O$ on the enhanced **2a** selectivity by suppressing further hydrogenation of **2a**. Previous research revealed that a competitive and prior adsorption of N_2H_4 over H_2 on the catalyst surface can reduce catalyst activity by inhibiting H_2 adsorption and activation [58–60]. Therefore, in our case, the observed high selectivity to **2a** by additionally introduced N_2H_4 in the hydrogenation system is actually at the expense of appropriately reduced catalyst activity, thus avoiding the further hydrogenation of **2a** to **7** (Fig. 8a).

In addition to intermediate **3**, direct hydrogenation of **4** was also investigated with Ru/BNC under pressurized H_2 . Fig. 8d shows the resulting complicated profiles of the reaction time vs. product distribution. **4** quickly hydrogenated at initial 4 h, then smoothly and slowly transformed with a full conversion after 16 h. **2a** yields steeply increased to 33% at initial 4 h with a quick decline of **4** concentrations, and then **2a** yields slowly raised to a maximum of 38% at 12 h. Further prolonged reaction time beyond this stage led to a decreased **2a** yield to 26% at 16 h. In contrast, **7** yields smoothly enhanced with reaction time and reached a maximum of 69% at 16 h with **2a** as a detected intermediate for **4**-to-**7** transformation (Fig. 8a,d). Notably, trace amount of secondary amine **9** (Fig. S7, Supporting Information) was observed in 1–4% yields during the hydrogenation (Fig. 8a,d). **9** should be obtained by

hydrogenation of Schiff base *N*-(2-furanylmethylene)-2-furanmethanamine (**8**) which is *in situ* formed by substitutions of **3/2a** or **4/2a** under the reaction conditions (Fig. 8a).

Similarly, to investigate the presence of $N_2H_4 \cdot H_2O$ on the **2a** selectivity, direct hydrogenation of **4** was performed in the existence of 4 equivalents of $N_2H_4 \cdot H_2O$ for comparison purpose (Fig. 8e). Interestingly, a quick reaction of **4** with N_2H_4 was observed at initial 0.5 h to afford **3** in 81% yield. The following **3**-to-**2a** transformation initiated beyond this time, **2a** yields then smoothly raised at the expense of the **3** concentrations giving a maximum of 99% yield **2a** after 20 h. Notably, both **7** and **9** were unobserved to any detectable extents. Therefore, additionally introduced N_2H_4 in the hydrogenative system of **4** can significantly enhance both selectivity and yield of **2a** by changing the reaction pathway with **3** as the observed reaction intermediate.

3.6. Effect of nitrogen source on furfurylamine selectivity

Previous research focused on nitrogen source of $NH_3 \cdot H_2O$ for the reductive amination of **1a** (Table S1). Therefore, the influence of nitrogen source on the reductive amination was investigated and compared by respectively using $N_2H_4 \cdot H_2O$, $NH_3 \cdot H_2O$ and hydroxylamine ($H_2NOH \cdot H_2O$) in the presence of Ru/BNC (Fig. 9a). $N_2H_4 \cdot H_2O$ afforded quantitative **2a** yield (>99%), showing an excellent selectivity for **1a**-to-**2a** transformation under the investigated conditions. In the case of $NH_3 \cdot H_2O$, 84% yield of **2a** was obtained with **6** (12% yield, Fig. S8, Supporting Information) and **9** (4% yield) as observed by-products (Fig. 9a,e). When $H_2NOH \cdot H_2O$ was examined as the nitrogen source, negligible **2a** yield (9%) was detected under the investigated conditions with **7** (91% yield) as the main product (Fig. 9a,e). Therefore, $N_2H_4 \cdot H_2O$ highlights an excellent selectivity and quantitative yield of the desired **2a** product for the reductive amination among various investigated nitrogen sources under the reaction conditions.

The mechanism for reductive amination of **1a** with NH_3 was proposed by reported literatures (Scheme 1a). In our case, Ru/BNC-promoted reductive amination of **1a** with $NH_3 \cdot H_2O$ as nitrogen source was further examined with the profiles of reaction time vs. product distribution (Fig. 9b), Fig. 9e shows the corresponding reaction network

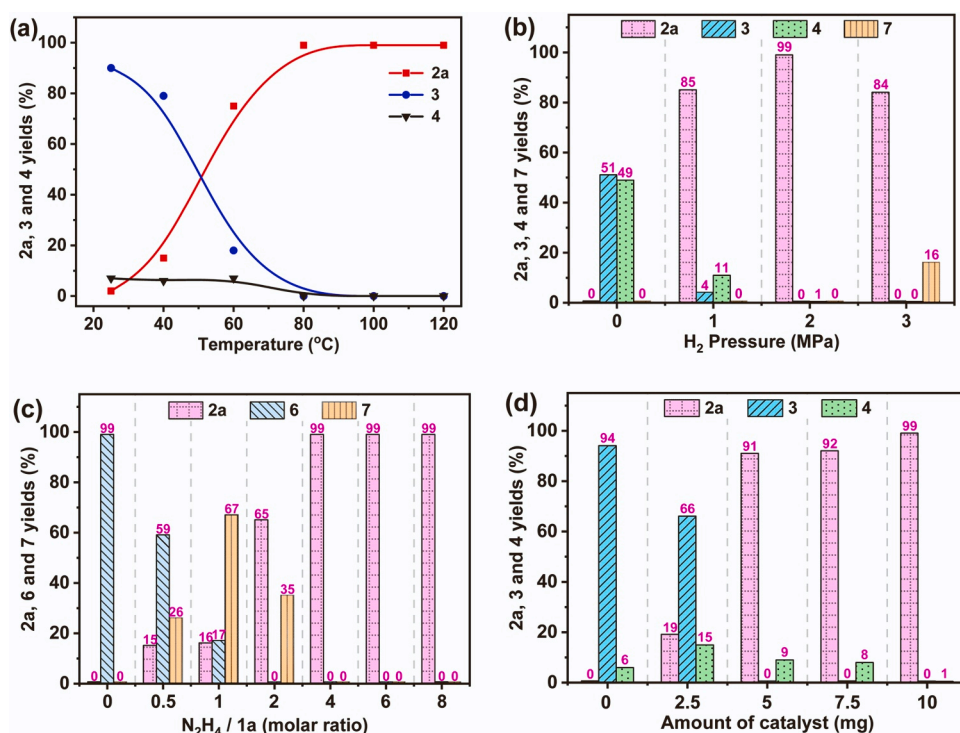


Fig. 10. Effect of (a) temperature, (b) initial H_2 pressure, (c) $N_2H_4/1a$ ratios, and (d) catalyst loading amount on the reductive amination of **1a** over Ru/BNC catalyst. Reaction conditions: (a) **1a** (0.12 mmol), Ru/BNC (10 mg, 1.8 wt% Ru, 1.1 mol% Ru relative to **1a**), $N_2H_4 \cdot H_2O$ (0.24 M in 2.0 mL MeOH, 4 equivalents to **1a**), H_2 (2.0 MPa), 16 h; (b) **1a** (0.12 mmol), Ru/BNC (10 mg), $N_2H_4 \cdot H_2O$ (0.24 M in 2.0 mL MeOH, 4 equivalents to **1a**), 80 °C, 16 h; (c) **1a** (0.12 mmol), Ru/BNC (10 mg), H_2 (2.0 MPa), 80 °C, 16 h; (d) **1a** (0.12 mmol), $N_2H_4 \cdot H_2O$ (0.24 M in 2.0 mL MeOH, 4 equivalents to **1a**), H_2 (2.0 MPa), 80 °C, 16 h.

of the reductive amination. **1a** fully converted at initial 0.5 h to give a mixture of Schiff base **8** (58%, Fig. S9, Supporting Information), **2a** (23%), **6** (15%) and **9** (4%) (Fig. 9b). Among these observed compounds, Schiff base **8** was detected as intermediate, initially and quickly formed, reached a maximum of 58% yield at 0.5 h, and then full consumed at 8 h. **2a** was obtained by direct hydrogenation of the C=N bond in the *in-situ* formed **5** (Figs. 9e), **2a** yield steeply increased to 67% at initial 2 h and then slowly reached a maximum of 84% after 8 h. **6** was obtained by direct hydrogenation of the carbonyl group (C=O bond) in **1a** (Fig. 9e). Generally, **6** formed at initial 0.5 h and kept a constant concentration (11~15%) after this time. **1a** amination to **5** and **1a** hydrogenation to **6** parallelly and competitively performed at the initial 0.5 h (Fig. 9b,e). Quick condensation of **1a** with the *in-situ* formed **2a** afforded Schiff base **8**. There are two reaction pathways for **8** transformation. One is the subsequent direct hydrogenation of **8**, yielding a negligible yield of **9** (3~5%). The other is the predominant pathway, which is **8**-to-**2a** transformation in the presence of excess amount of NH_3 via a successive aminolysis/hydrogenolysis with *gem*-diamine (**10**, Fig. 9e) as the proposed intermediate.

In the case of $\text{H}_2\text{NOH}\cdot\text{H}_2\text{O}$ as the nitrogen source, **1a** was completely converted after initial 1 h, giving a maximum **2a** yield of 95% at this stage (Fig. 9c). Further prolonged reaction time beyond this stage led to a deep hydrogenation of **2a** to **7**, giving 98% yield of **7** at 20 h. Fig. 9e shows the resulting network of the reductive amination of **1a** with $\text{H}_2\text{NOH}\cdot\text{H}_2\text{O}$. Notably, furfuraldehyde oxime (**17**, Fig. 9e) was undetected under the reaction condition, presumably due to its high reactivity.

To further probe the effect of competition between various nitrogen sources on the product selectivity, a mixture of $\text{NH}_3\cdot\text{H}_2\text{O}$ (2 equivalents to **1a**) and $\text{N}_2\text{H}_4\cdot\text{H}_2\text{O}$ (2 equivalents to **1a**) was investigated as a mixed nitrogen sources for **1a** reductive amination with Ru/BNC catalyst. Interestingly, the resulting profiles (Fig. 9d) of reaction time vs. product were very close to those of the **1a** reductive amination with $\text{N}_2\text{H}_4\cdot\text{H}_2\text{O}$ (4 equivalents) alone (Fig. 7b). However, a quantitative **2a** yield (>99%) was obtained by a prolonged reaction time to 24 h. Moreover, a reduced molar ratio of 3/4 was observed in the profile due to a reduced $\text{N}_2\text{H}_4\cdot\text{H}_2\text{O}$ loading level to **1a** (Figs. 7b and 9d). The *in-situ* formed **3** (in 90% yield) initially underwent hydrogenation/hydrogenolysis to **2a** with a full conversion at 16 h to yield **2a** in 74%. Subsequent hydrogenation/hydrogenolysis of **4** to **2a** initiated beyond this time, finally affording **2a** in 99% yield at 24 h. The above results further suggested a more ready transformation of the monohydrazone **3** to **2a** when compared with dihydrazone **4**. Notably, $\text{NH}_3\cdot\text{H}_2\text{O}$ -induced by-products such as **6**, **8** and **9** were unobserved in the mixed nitrogen sources of $\text{NH}_3\text{--N}_2\text{H}_4$. Evidently, **1a** favored direct condensation with N_2H_4 in the mixture of $\text{NH}_3\text{--N}_2\text{H}_4$, the reductive amination performed through the hydrazone intermediates **3** and **4** rather than **5**. The mixed-nitrogen source experiment further suggested the superiority of the $\text{N}_2\text{H}_4\cdot\text{H}_2\text{O}$ on the selective reductive amination for **2a** formation.

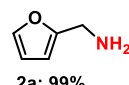
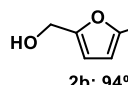

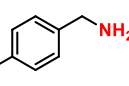
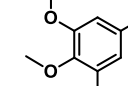
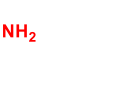
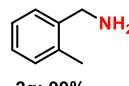
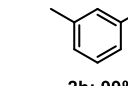
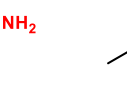
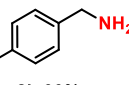
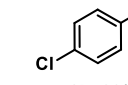
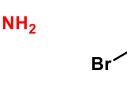
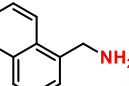
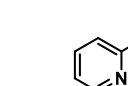
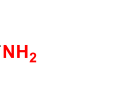
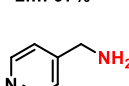
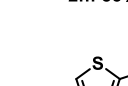

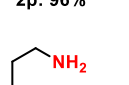
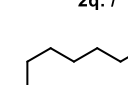
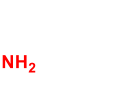
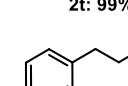
3.7. Controlled experiments

Various reaction parameters such as reaction temperature, initial H_2 pressure, molar ratio of $\text{N}_2\text{H}_4\cdot\text{H}_2\text{O}$ to **1a**, and catalyst amount were examined with the Ru/BNC-promoted reductive amination. The reaction temperature on the reductive amination demonstrated that both **3** and **4** were immediately and quantitatively formed in a combined yield of 97% even at ambient reaction temperature (Fig. 10a). While, negligible **2a** yield (2%) was observed at ambient temperature, suggesting a key role of temperature on the 3/4-hydrogenation if compared with **1a**-condensation with N_2H_4 . Increasing reaction temperature significantly promoted the hydrogenation to afford **2a**, a maximum of 99% yield of **2a** was observed at 80 °C with full conversions of both **3** and **4**. Side reactions and by-products were unobserved to any detectable extents even by increasing the reaction temperature to 120 °C.

As a reducing agent for the reductive amination, the influence of

Table 2

Ru/BNC- $\text{N}_2\text{H}_4\cdot\text{H}_2\text{O}$ system promoted reductive amination of various aldehydes for primary amines syntheses.^a

$\text{R-CHO} + \text{N}_2\text{H}_4\cdot\text{H}_2\text{O} + \text{H}_2 \xrightarrow[\text{MeOH, 80 °C, 16 h}]{\text{Ru/BNC}} \text{R-CH}_2\text{NH}_2$		
1		2
		
2a: 99%	2b: 94%	2c: 99%
		
2d: 99%	2e: 99%	2f: 99%
		
2g: 99%	2h: 99%	2i: 94%
		
2j: 99%	2k: 99%	2l: 95%
		
2m: 97%	2n: 85%	2o: 89%
		
2p: 96%	2q: /	2r: 98%
		
2s: 97%	2t: 99%	2u: 88%
		
	2v: 99%	

^aReaction conditions: aldehyde **1** (0.12 mmol), Ru/BNC (10 mg, 1.8 wt% Ru, 1.1 mol% Ru relative to **1**), $\text{N}_2\text{H}_4\cdot\text{H}_2\text{O}$ (0.24 M in 2.0 mL MeOH, 4 equivalents to **1**), H_2 (2.0 MPa), 80 °C, 16 h.

initial H_2 pressure on the reaction demonstrated that only the hydrazone type intermediates of **3** and **4** were detected in the reaction system in the absence of H_2 (Fig. 10b). Therefore, the hydrogenation cannot perform without H_2 . Moreover, our controlled experiments demonstrated that excess amount N_2H_4 in the reaction system cannot function as hydrogen source for transfer hydrogenation of **3/4** to **2a** with the Ru/BNC catalyst under N_2 atmosphere. Increasing H_2 pressure to 1.0 MPa led to a steeply increased **2a** yield to 85%, and 99% yield of **2a** was obtained by 2.0 MPa H_2 . Further raising H_2 pressure to 3.0 MPa resulted in a reduced **2a** yield to 84% due to subsequent hydrogenation of furan-ring in **2a** to give **7**.

The influence of $\text{N}_2\text{H}_4/1\text{a}$ molar ratio on the reductive amination revealed that **1a** was completely hydrogenated to **6** in the absence of $\text{N}_2\text{H}_4\cdot\text{H}_2\text{O}$, suggesting a key role of N_2H_4 as a nitrogen source (Fig. 10c).

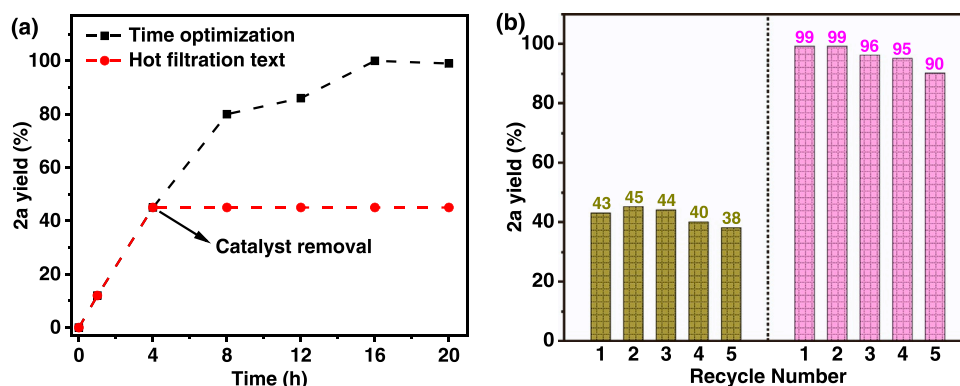


Fig. 11. Reductive amination of **1a** to **2a** over Ru/BNC: (a) hot filtration test and (b) catalyst recycling experiments at different conversion levels. Reaction conditions: **1a** (0.12 mmol), Ru/BNC (10 mg, 1.8 wt% Ru, 1.1 mol% Ru relative to **1a**), $\text{N}_2\text{H}_4\cdot\text{H}_2\text{O}$ (0.24 M in 2.0 mL MeOH, 4 equivalents to **1a**), H_2 (2.0 MPa), 80 °C. **2a** yields were respectively obtained at 4 h (left) and 16 h (right) in the Fig. 11(b).

Increasing the $\text{N}_2\text{H}_4/\mathbf{1a}$ ratio, on the one hand, promoted amination reaction by inhibiting direct hydrogenation of **1a** to **6**. On the other hand, enhanced N_2H_4 loading level efficiently increased **2a** selectivity by suppressing subsequent **2a** hydrogenation to **7**. **2a** yields remarkably increased to 99% with an optimal $\text{N}_2\text{H}_4/\mathbf{1a}$ molar ratio of 4. Further increasing the molar ratio to 8 had no effect on **2a** yields.

The influence of catalyst loading amount on the reductive amination suggested that **2a** yields smoothly enhance to 99% with Ru/BNC amount increasing to 10 mg (Fig. 10d), suggesting a promotion effect for the accessibility and availability of catalytic Ru sites in the reaction. Therefore, an optimized 99% yield of **2a** was observed under the reaction temperature of 80 °C with 2.0 MPa of H_2 and 4 equivalents of $\text{N}_2\text{H}_4\cdot\text{H}_2\text{O}$ to **1a** by using Ru/BNC catalyst in methanol. The optimized conditions were then extended to various aldehydes for the corresponding primary amines syntheses *via* the developed reductive amination methods.

3.8. Scope of the reductive amination

The scope of aldehydes in the reductive amination was then probed by using the catalytic system of Ru/BNC– N_2H_4 (Table 2). For biomass-based aldehydes such as furfural (**1a**), 5-hydroxymethylfurfural (**1b**), 5-methylfurfural (**1c**), 4-methoxybenzaldehyde (**1d**) and 3,4,5-trimethoxybenzaldehyde (**1e**), the resulting primary amines (**2a–e**) were quantitatively synthesized in 94–99% yields. Moreover, the Ru/BNC– N_2H_4 system was also applicable to various fossil resource-based aldehydes for the reductive amination. For example, aromatic aldehyde of benzaldehyde (**1f**) was reductively aminated to benzylamine (**2f**) in 99% yield. Moreover, substituted **1f**, bearing electron-donating ($-\text{CH}_3$; **1g–i**) and

electron-withdrawing ($-\text{F}$, $-\text{Cl}$, $-\text{Br}$; **1j–l**) groups, were well tolerated under the investigated conditions, producing the desired substituted benzylamines (**2g–l**) in excellent yields (94–99%). Notably, dehalogenation was unobserved with halogen-substituted **1f** during the reductive amination (**2j–l**). Surprisingly, bulky 1-naphthaldehyde (**1m**) was transformed into the 1-naphthalenemethylamine (**2m**) in 97% yield, suggesting a well tolerance of the reductive amination system to steric hindrance substrate. In addition, heterocyclic aromatic aldehydes of pyridinylaldehydes (**1n–p**) were well compatible with the current catalytic system. However, 2-thiophenecarboxaldehyde (**1q**) failed to give the corresponding 2-thiophenylmethanamine (**2q**) under the investigated conditions with, however, quantitative 1,2-bis(2-thiophenylmethylene)hydrazine (Fig. S10, Supporting Information) as the observed product. The above result suggested a poisoning effect of S atom in **1q** on the Ru catalyst. Finally, aliphatic aldehydes such as *n*-butyl aldehyde (**1r**), *n*-hexaldehyde (**1s**), lauraldehyde (**1t**), cyclohexanecarboxaldehyde (**1u**), and 3-phenylpropionaldehyde (**1v**) can be well reductively aminated to give the desired primary amines (**2r–v**) in

high yield (88–99%). These results thus clearly indicated a high efficiency of the developed catalytic system Ru/BNC– N_2H_4 for transformation of a wide range of aldehydes to the desired primary amines *via* the reductive amination.

3.9. Catalyst reusability

Catalyst stability and recycling performance are essential in industrial applications. A hot filtration experiment was then performed for **1a**-to-**2a** transformation to demonstrate the heterogeneity of the Ru/BNC. The reaction was carried out under the optimal conditions and quenched at 4 h with **2a** yield of 45%, the Ru/BNC was then removed from the hot reaction mixture (Fig. 11a). The resulting mother liquor was allowed to stir alone for the remaining 16 h under the identical conditions; however, no further reaction was observed. Inductively coupled plasma-atomic emission spectroscopy (ICP-AES) analysis indicated no leaching of Ru species in the mother liquor based on the detection limitation. The hot filtration experiment thus suggested the heterogeneous nature of the Ru/BNC catalyst.

The Ru/BNC reusability was further evaluated by a five-time consecutive run for **1a**-to-**2a** transformation. The recovered Ru/BNC was separated by centrifugation from the reaction mixture and subjected to the next cycling. Fig. 11b shows a ready reuse of Ru/BNC catalyst over five cycles without significant decay in **2a** yield, indicating the excellent recyclability. The recovered Ru/BNC catalyst after five cycles was systematically analyzed by XRD, XPS, TEM, and N_2 sorption analysis. Our XRD and XPS results showed almost unchanged crystal structure and surface electronic structure of the recover Ru/BNC, thus indicating its good durability (Fig. S11 and Table S2, Supporting Information). However, the spent Ru/BNC exhibited a slight decline of specific surface area when compared with fresh sample (Table 1 and Fig. S12, Supporting Information). This observation was presumably attributed to the strong adsorption of hydrazone species on the surface of recover Ru/BNC, leading to the pore blockage. Moreover, our TEM analysis demonstrated an increased mean Ru NPs size from 1.1 nm for fresh Ru/BNC to 2.2 nm for recover sample (Fig. S12). Therefore, a slightly decreased activity of the catalyst during the recycling experiment can presumably be related to the strong adsorption of hydrazone intermediates on the catalyst surface and slight sintering/agglomeration of Ru NPs on the catalyst surface.

4. Conclusions

In summary, a highly efficient and selective approach to biomass-based amine was achieved by reductive amination of furfural with hydrous hydrazine using Ru/BNC catalyst. The rich FLPs on the BNC surface synergistically enhanced the activity of Ru catalyst, producing

quantitative **2a** yield. While, quick formation rate of hydrazone intermediate and its moderate reactivity significantly improved **2a** selectivity in the **1a**/ N_2H_4 -to-**2a** transformation. Additionally, the developed Ru/BNC- N_2H_4 system was applicable to a wide range of aldehydes to give the corresponding primary amines in excellent to good yields via the reductive amination.

CRedit authorship contribution statement

Hongtao Zou developed the catalytic method and performed the experiments. **Jinzu Chen** designed and directed the investigations. All the authors were involved in the analysis of results, discussions of project, and composition of manuscript.

Declaration of Competing Interest

The authors declare that they have no known competing financial interests or personal relationships that could have appeared to influence the work reported in this paper.

Acknowledgments

This work was supported by the National Natural Science Foundation of China (22075104), the Youth Science and Technology Innovation Talent of Guangdong TeZhi Plan (2019TQ05L111), and Educational Commission of Guangdong Province of China (2021ZDZX4037, 2021KCXTD009).

Appendix A. Supporting information

Supplementary data associated with this article can be found in the online version at doi:10.1016/j.apcatb.2022.121262.

References

- [1] G. Liang, A. Wang, L. Li, G. Xu, N. Yan, T. Zhang, Production of primary amines by reductive amination of biomass-derived aldehydes/ketones, *Angew. Chem. Int. Ed.* 56 (2017) 3050–3054, <https://doi.org/10.1002/anie.201610964>.
- [2] G. Hahn, P. Kunas, N. de Jonge, R. Kempe, General synthesis of primary amines via reductive amination employing a reusable nickel catalyst, *Nat. Catal.* 2 (2018) 71–77, <https://doi.org/10.1038/s41929-018-0202-6>.
- [3] V. Froidevaux, C. Negrell, S. Caillol, J.P. Pascault, B. Boutevin, Biobased amines: from synthesis to polymers; present and future, *Chem. Rev.* 116 (2016) 14181–14224, <https://doi.org/10.1021/acs.chemrev.6b00486>.
- [4] X.-P. Fu, P. Han, Y.-Z. Wang, S. Wang, N. Yan, Insight into the roles of ammonia during direct alcohol amination over supported Ru catalysts, *J. Catal.* 399 (2021) 121–131, <https://doi.org/10.1016/j.jcat.2021.05.002>.
- [5] L. Fang, Z. Yan, J. Wu, A. Bugaev, C. Lamberti, M. Pera-Titus, Highly selective Ru/HBEA catalyst for the direct amination of fatty alcohols with ammonia, *Appl. Catal. B Environ.* 286 (2021), 119942, <https://doi.org/10.1016/j.apcatb.2021.119942>.
- [6] R.V. Jagadeesh, K. Murugesan, A.S. Alshammari, H. Neumann, M.M. Pohl, J. Radnik, M. Beller, MOF-derived cobalt nanoparticles catalyze a general synthesis of amines, *Science* 358 (2017) 326–332, <https://doi.org/10.1126/science.aan6245>.
- [7] K. Murugesan, T. Sentharamai, V.G. Chandrashekar, K. Natte, P.C.J. Kamer, M. Beller, R.V. Jagadeesh, Catalytic reductive aminations using molecular hydrogen for synthesis of different kinds of amines, *Chem. Soc. Rev.* 49 (2020) 6273–6328, <https://doi.org/10.1039/c9cs00286c>.
- [8] H. Qi, J. Yang, F. Liu, L. Zhang, J. Yang, X. Liu, L. Li, Y. Su, Y. Liu, R. Hao, A. Wang, T. Zhang, Highly selective and robust single-atom catalyst Ru₁/NC for reductive amination of aldehydes/ketones, *Nat. Commun.* 12 (2021) 3295, <https://doi.org/10.1038/s41467-021-23429-w>.
- [9] C. Xie, J. Song, M. Hua, Y. Hu, X. Huang, H. Wu, G. Yang, B. Han, Ambient-temperature synthesis of primary amines via reductive amination of carbonyl compounds, *ACS Catal.* 10 (2020) 7763–7772, <https://doi.org/10.1021/acscatal.0c01872>.
- [10] J. Lv, Y. Shen, L. Peng, X. Guo, W. Ding, Exclusively selective oxidation of toluene to benzaldehyde on ceria nanocubes by molecular oxygen, *Chem. Commun.* 46 (2010) 5909–5911, <https://doi.org/10.1039/c0cc00777c>.
- [11] T. Li, F. Chen, R. Lang, H. Wang, Y. Su, B. Qiao, A. Wang, T. Zhang, Styrene hydroformylation with in situ hydrogen: regioselectivity control by coupling with the low-temperature water-gas shift reaction, *Angew. Chem. Int. Ed.* 59 (2020) 7430–7434, <https://doi.org/10.1002/anie.202000998>.
- [12] C. Xu, E. Paone, D. Rodriguez-Padron, R. Luque, F. Mauriello, Recent catalytic routes for the preparation and the upgrading of biomass derived furfural and 5-hydroxymethylfurfural, *Chem. Soc. Rev.* 49 (2020) 4273–4306, <https://doi.org/10.1039/d0cs00041h>.
- [13] A. Takagaki, M. Takahashi, S. Nishimura, K. Ebitani, One-pot synthesis of 2,5-diformylfuran from carbohydrate derivatives by sulfonated resin and hydrothermalite-supported ruthenium catalysts, *ACS Catal.* 1 (2011) 1562–1565, <https://doi.org/10.1021/cs200456t>.
- [14] M. Fache, B. Boutevin, S. Caillol, Vanillin production from lignin and its use as a renewable chemical, *ACS Sustain. Chem. Eng.* 4 (2015) 35–46, <https://doi.org/10.1021/acssuschemeng.5b01344>.
- [15] H. Ishikawa, M. Sheng, A. Nakata, K. Nakajima, S. Yamazoe, J. Yamasaki, S. Yamaguchi, T. Mizugaki, T. Mitsudome, Air-stable and reusable cobalt phosphide nanoalloy catalyst for selective hydrogenation of furfural derivatives, *ACS Catal.* 11 (2021) 750–757, <https://doi.org/10.1021/acscatal.0c03300>.
- [16] J.D. Vidal, M.J. Climent, P. Concepcion, A. Corma, S. Iborra, M.J. Sabater, Chemicals from biomass: chemoselective reductive amination of ethyl levulinate with amines, *ACS Catal.* 5 (2015) 5812–5821, <https://doi.org/10.1021/acscatal.5b01113>.
- [17] V. Boosa, S. Varimalla, M. Dumpalappally, N. Gutta, V.K. Velisoju, N. Nama, V. Akula, Influence of Brønsted acid sites on chemoselective synthesis of pyrrolidones over H-ZSM-5 supported copper catalyst, *Appl. Catal. B Environ.* 292 (2021), 120177, <https://doi.org/10.1016/j.apcatb.2021.120177>.
- [18] A. Dumbabin, F. Subrizi, J.M. Ward, T.D. Sheppard, H.C. Hailes, Furfurylamines from biomass: transaminase catalysed upgrading of furfurals, *Green. Chem.* 19 (2017) 397–404, <https://doi.org/10.1039/c6gc02241c>.
- [19] C. Dong, H. Wang, H. Du, J. Peng, Y. Cai, S. Guo, J. Zhang, C. Smart, M. Ding, Ru/HZSM-5 as an efficient and recyclable catalyst for reductive amination of furfural to furfurylamine, *Mol. Catal.* 482 (2020), 110755, <https://doi.org/10.1016/j.mcat.2019.110755>.
- [20] N.S. Gould, H. Landfield, B. Dinkelacker, C. Brady, X. Yang, B. Xu, Selectivity control in catalytic reductive amination of furfural to furfurylamine on supported catalysts, *ChemCatChem* 12 (2020) 2106–2115, <https://doi.org/10.1002/cctc.201901662>.
- [21] T. Komanoya, T. Kinemura, Y. Kita, K. Kamata, M. Hara, Electronic effect of ruthenium nanoparticles on efficient reductive amination of carbonyl compounds, *J. Am. Chem. Soc.* 139 (2017) 11493–11499, <https://doi.org/10.1021/jacs.7b04481>.
- [22] D. Chandra, Y. Inoue, M. Sasase, M. Kitano, A. Bhaumik, K. Kamata, H. Hosono, M. Hara, A high performance catalyst of shape-specific ruthenium nanoparticles for production of primary amines by reductive amination of carbonyl compounds, *Chem. Sci.* 9 (2018) 5949–5956, <https://doi.org/10.1039/c8sc01197d>.
- [23] D. Deng, Y. Kita, K. Kamata, M. Hara, Low-temperature reductive amination of carbonyl compounds over Ru deposited on Nb₂O₅-nH₂O, *ACS Sustain. Chem. Eng.* 7 (2018) 4692–4698, <https://doi.org/10.1021/acssuschemeng.8b04324>.
- [24] T. Sentharamai, K. Murugesan, J. Schneidewind, N.V. Kalevaru, W. Baumann, H. Neumann, P.C.J. Kamer, M. Beller, R.V. Jagadeesh, Simple ruthenium-catalyzed reductive amination enables the synthesis of a broad range of primary amines, *Nat. Commun.* 9 (2018) 4123, <https://doi.org/10.1038/s41467-018-06416-6>.
- [25] W. Guo, T. Tong, X. Liu, Y. Guo, Y. Wang, Morphology-Tuned Activity of Ru/Nb₂O₅ Catalysts for Ketone Reductive Amination, *ChemCatChem* 11 (16) (2019) 4130–4138.
- [26] M. Chatterjee, T. Ishizaka, H. Kawanami, Reductive amination of furfural to furfurylamine using aqueous ammonia solution and molecular hydrogen: an environmentally friendly approach, *Green. Chem.* 18 (2016) 487–496, <https://doi.org/10.1039/c5gc01352f>.
- [27] X. Jv, S. Sun, Q. Zhang, M. Du, L. Wang, B. Wang, Efficient and mild reductive amination of carbonyl compounds catalyzed by dual-function palladium nanoparticles, *ACS Sustain. Chem. Eng.* 8 (2019) 1618–1626, <https://doi.org/10.1021/acssuschemeng.9b06464>.
- [28] K. Zhou, B. Chen, X. Zhou, S. Kang, Y. Xu, J. Wei, Selective synthesis of furfurylamine by reductive amination of furfural over raney cobalt, *ChemCatChem* 11 (2019) 5562–5569, <https://doi.org/10.1002/cctc.201901269>.
- [29] M. Sheng, S. Fujita, S. Yamaguchi, J. Yamasaki, K. Nakajima, S. Yamazoe, T. Mizugaki, T. Mitsudome, Single-crystal cobalt phosphide nanorods as a high-performance catalyst for reductive amination of carbonyl compounds, *JACS Au* 1 (2021) 501–507, <https://doi.org/10.1021/jacsau.1c00125>.
- [30] M. Manzoli, E.C. Gaudino, G. Cravotto, S. Tabasso, R.B.N. Baig, E. Colacino, R. S. Varma, Microwave-assisted reductive amination with aqueous ammonia: sustainable pathway using recyclable magnetic nickel-based nanocatalyst, *ACS Sustain. Chem. Eng.* 7 (2019) 5963–5974, <https://doi.org/10.1021/acssuschemeng.8b06054>.
- [31] L. Lv, L. Yu, Z. Qiu, C.J. Li, Switch in selectivity for formal hydroalkylation of 1,3-dienes and enynes with simple hydrazones, *Angew. Chem. Int. Ed.* 59 (2020) 6466–6472, <https://doi.org/10.1002/anie.201915875>.
- [32] Z. Qiu, L. Lv, J. Li, C.C. Li, C.J. Li, Direct conversion of phenols into primary anilines with hydrazine catalyzed by palladium, *Chem. Sci.* 10 (2019) 4775–4781, <https://doi.org/10.1039/c9sc00595a>.
- [33] D.W. Stephan, G. Erker, Frustrated Lewis pairs: metal-free hydrogen activation and more, *Angew. Chem. Int. Ed.* 49 (2010) 46–76, <https://doi.org/10.1002/anie.200903708>.
- [34] Y. Ding, X. Huang, X. Yi, Y. Qiao, X. Sun, A. Zheng, D.S. Su, A heterogeneous metal-free catalyst for hydrogenation: Lewis acid-base pairs integrated into a carbon lattice, *Angew. Chem. Int. Ed.* 57 (2018) 13800–13804, <https://doi.org/10.1002/anie.201803977>.
- [35] S. Zhong, N. Tsumori, M. Kitta, Q. Xu, Immobilizing palladium nanoparticles on boron-oxygen-functionalized carbon nanospheres towards efficient hydrogen

- generation from formic acid, *Nano Res.* 12 (2019) 2966–2970, <https://doi.org/10.1007/s12274-019-2539-9>.
- [36] H. Zou, Q. Yao, M. Huang, M. Zhu, F. Zhang, Z.-H. Lu, Noble-metal-free NiFe nanoparticles immobilized on nano CeZrO₂ solid solutions for highly efficient hydrogen production from hydrous hydrazine, *Sustain. Energy Fuels* 3 (2019) 3071–3077, <https://doi.org/10.1039/C9SE00547A>.
- [37] C. Lin, W. Wan, X. Wei, J. Chen, H₂ activation with Co nanoparticles encapsulated in N-doped carbon nanotubes for green synthesis of benzimidazoles, *ChemSusChem* 14 (2021) 709–720, <https://doi.org/10.1002/cssc.202002344>.
- [38] Z. Ye, J. Chen, Sulfonate-grafted metal–organic frameworks for reductive functionalization of CO₂ to benzimidazoles and N-formamides, *ACS Catal.* 11 (2021) 13983–13999, <https://doi.org/10.1021/acscatal.1c03329>.
- [39] C. Zhang, F. Han, Hollow Ru nanoparticles for electrocatalytic hydrogen evolution, *ACS Appl. Nano Mater.* 4 (2021) 8530–8538, <https://doi.org/10.1021/acsnano.1c01847>.
- [40] L. Yang, D. Wu, T. Wang, D. Jia, B/N-codoped carbon nanosheets derived from the self-assembly of chitosan-amino acid gels for greatly improved supercapacitor performances, *ACS Appl. Mater. Interfaces* 12 (2020) 18692–18704, <https://doi.org/10.1021/acsami.0c01655>.
- [41] H. Chen, Y. Xiong, T. Yu, P. Zhu, X. Yan, Z. Wang, S. Guan, Boron and nitrogen co-doped porous carbon with a high concentration of boron and its superior capacitive behavior, *Carbon* 113 (2017) 266–273, <https://doi.org/10.1016/j.carbon.2016.11.035>.
- [42] P. Gogoi, N. Kanna, P. Begum, R.C. Deka, S.C.V. V, T. Raja, Controlling and stabilization of Ru nanoparticles by tuning the nitrogen content of the support for enhanced H₂ production through aqueous-phase reforming of glycerol, *ACS Catal.* 10 (2019) 2489–2507, <https://doi.org/10.1021/acscatal.9b04063>.
- [43] C. Van Nguyen, S. Lee, Y.G. Chung, W.-H. Chiang, K.C.W. Wu, Synergistic effect of metal-organic framework-derived boron and nitrogen heteroatom-doped three-dimensional porous carbons for precious-metal-free catalytic reduction of nitroarenes, *Appl. Catal. B Environ.* 257 (2019), 117888 <http://doi.org/j.apcatb.2019.117888>.
- [44] X. Li, L. Ye, Z. Ye, S. Xie, Y. Qiu, F. Liao, C. Lin, M. Liu, N. P co-doped core/shell porous carbon as a highly efficient peroxymonosulfate activator for phenol degradation, *Sep. Purif. Technol.* 276 (2021), 119286 <http://doi.org/j.seppur.2021.119286>.
- [45] Z. Liu, X. Yang, G. Hu, L. Feng, Ru nanoclusters coupled on Co/N-doped carbon nanotubes efficiently catalyzed the hydrogen evolution reaction, *ACS Sustain. Chem. Eng.* 8 (2020) 9136–9144, <https://doi.org/10.1021/acsschemeng.0c02636>.
- [46] H. Li, M. Zhang, L. Yi, Y. Liu, K. Chen, P. Shao, Z. Wen, Ultrafine Ru nanoparticles confined in 3D nitrogen-doped porous carbon nanosheet networks for alkali-acid Zn-H₂ hybrid battery, *Appl. Catal. B: Environ.* 280 (2021), 119412, <https://doi.org/10.1016/j.apcatb.2020.119412>.
- [47] S.Y. Kim, J. Park, H.C. Choi, J.P. Ahn, J.Q. Hou, H.S. Kang, X-ray photoelectron spectroscopy and first principles calculation of BCN nanotubes, *J. Am. Chem. Soc.* 129 (2007) 1705–1716, <https://doi.org/10.1021/ja067592r>.
- [48] Y. Zhao, L. Yang, S. Chen, X. Wang, Y. Ma, Q. Wu, Y. Jiang, W. Qian, Z. Hu, Can boron and nitrogen co-doping improve oxygen reduction reaction activity of carbon nanotubes? *J. Am. Chem. Soc.* 135 (2013) 1201–1204, <https://doi.org/10.1021/ja310566z>.
- [49] S. Liang, H.-Y. Niu, H. Guo, C.-G. Niu, C. Liang, J.-S. Li, N. Tang, L.-S. Lin, C.-W. Zheng, Incorporating Fe₃C into B, N co-doped CNTs: non-radical-dominated peroxymonosulfate catalytic activation mechanism, *Chem. Eng. J.* 405 (2021), 126686, <https://doi.org/10.1016/j.cej.2020.126686>.
- [50] Z. Xie, X. Shang, J. Yang, B. Hu, P. Nie, W. Jiang, J. Liu, 3D interconnected boron- and nitrogen-codoped carbon nanosheets decorated with manganese oxides for high-performance capacitive deionization, *Carbon* 158 (2020) 184–192, <https://doi.org/10.1016/j.carbon.2019.12.004>.
- [51] M.S. Kim, S. Cho, S.H. Joo, J. Lee, S.K. Kwak, M.I. Kim, J. Lee, N- and B-codoped graphene: a strong candidate to replace natural peroxidase in sensitive and selective bioassays, *ACS Nano* 13 (2019) 4312–4321, <https://doi.org/10.1021/acsnano.8b09519>.
- [52] Y. Wu, Z. Gao, Y. Feng, Q. Cui, C. Du, C. Yu, L. Liang, W. Zhao, J. Feng, J. Sun, R. Yang, J. Sun, Harnessing selective and durable electrosynthesis of H₂O₂ over dual-defective yolk-shell carbon nanosphere toward on-site pollutant degradation, *Appl. Catal. B Environ.* 298 (2021), 120572, <https://doi.org/10.1016/j.apcatb.2021.120572>.
- [53] R.Y. Tay, H. Li, S.H. Tsang, M. Zhu, M. Loeblein, L. Jing, F.N. Leong, E.H.T. Teo, Trimethylamine borane: a new single-source precursor for monolayer h-BN single crystals and h-BCN thin films, *Chem. Mater.* 28 (2016) 2180–2190, <https://doi.org/10.1021/acs.chemmater.6b00114>.
- [54] G.C. Welch, R.R.S. Juan, J.D. Masuda, D.W. Stephan, Reversible, metal-free hydrogen activation, *Science* 314 (2006) 1124–1126, <https://doi.org/10.1126/science.1134230>.
- [55] D.W. Stephan, G. Erker, Frustrated Lewis pair chemistry: development and perspectives, *Angew. Chem. Int. Ed.* 54 (2015) 6400–6441, <https://doi.org/10.1002/anie.201409800>.
- [56] A. Primo, F. Neatu, M. Florea, V. Parvulescu, H. Garcia, Graphenes in the absence of metals as carbocatalysts for selective acetylene hydrogenation and alkene hydrogenation, *Nat. Commun.* 5 (2014) 5291, <https://doi.org/10.1038/ncomms6291>.
- [57] X. Chen, Q. Shen, Z. Li, W. Wan, J. Chen, J. Zhang, Metal-free H₂ activation for highly selective hydrogenation of nitroaromatics using phosphorus-doped carbon nanotubes, *ACS Appl. Mater. Interfaces* 12 (2020) 654–666, <https://doi.org/10.1021/acsami.9b17582>.
- [58] C. Zhang, H. Liu, Y. Liu, X. Liu, Y. Mi, R. Guo, J. Sun, H. Bao, J. He, Y. Qiu, J. Ren, X. Yang, J. Luo, G. Hu, Rh₂S₃/N-doped carbon hybrids as pH-universal bifunctional electrocatalysts for energy-saving hydrogen evolution, *Small Methods* 4 (2020), 2000208, <https://doi.org/10.1002/smt.202000208>.
- [59] T.D. Daff, N.H. de Leeuw, Ab initio molecular dynamics simulations of the cooperative adsorption of hydrazine and water on copper surfaces: implications for shape control of nanoparticles, *Chem. Mater.* 23 (2011) 2718–2728, <https://doi.org/10.1021/cm103164w>.
- [60] A.V. Ananiev, J.C. Broudic, P. Brossard, The platinum catalyzed hydrazine decomposition in non-nitrate acidic media, *Appl. Catal. A Gen.* 242 (2003) 1–10, [https://doi.org/10.1016/S0926-860X\(02\)00368-X](https://doi.org/10.1016/S0926-860X(02)00368-X).